



**Please cite the Published Version**

Alasali, Feras , El-Naily, Naser , Loukil, Hassen , Omran, Emad El Deen, Holderbaum, William , Elhaffar, Abdelsalam and Saidi, Abdelaziz Salah  (2024) The Performance and Robustness of Power Protection Schemes for GridConnected PV Systems Under Varied Smart Inverter Controllers. International Journal of Energy Research, 2024. 6805410 ISSN 0363-907X

**DOI:** <https://doi.org/10.1155/2024/6805410>

**Publisher:** Wiley

**Version:** Published Version

**Downloaded from:** <https://e-space.mmu.ac.uk/636841/>

**Usage rights:**  [Creative Commons: Attribution 4.0](https://creativecommons.org/licenses/by/4.0/)

**Additional Information:** This is an open access article which first appeared in International Journal of Energy Research

**Data Access Statement:** Derived data supporting the findings of this study are available from the corresponding author upon request.

**Enquiries:**

If you have questions about this document, contact [openresearch@mmu.ac.uk](mailto:openresearch@mmu.ac.uk). Please include the URL of the record in e-space. If you believe that your, or a third party's rights have been compromised through this document please see our Take Down policy (available from <https://www.mmu.ac.uk/library/using-the-library/policies-and-guidelines>)

Research Article

# The Performance and Robustness of Power Protection Schemes for Grid-Connected PV Systems Under Varied Smart Inverter Controllers

Feras Alasali <sup>1</sup>, Naser El-Naily <sup>2</sup>, Hassen Loukil <sup>3</sup>, Emad El Deen Omran,<sup>4</sup>  
William Holderbaum <sup>5</sup>, Abdelsalam Elhaffar,<sup>6</sup> and Abdelaziz Salah Saidi <sup>7</sup>

<sup>1</sup>Department of Electrical Engineering, Faculty of Engineering, The Hashemite University, P.O. Box 330127, Zarqa 13133, Jordan

<sup>2</sup>College of Electrical and Electronics Technology-Benghazi, Benghazi, Libya

<sup>3</sup>Department of Electrical Engineering, College of Engineering, King Khalid University, Abha 61421, Saudi Arabia

<sup>4</sup>Engineering Department, Suez Canal Authority, Ismailia, Egypt

<sup>5</sup>Science and Engineering, Manchester Metropolitan University, M1 5GD, Manchester, UK

<sup>6</sup>Department of Electrical Engineering, Sultan Qaboos University, Seeb, Oman

<sup>7</sup>National School of Engineers of Tunis, Electrical Systems Laboratory, University of Tunis El Manar, Tunis, Tunisia

Correspondence should be addressed to William Holderbaum; [w.holderbaum@mmu.ac.uk](mailto:w.holderbaum@mmu.ac.uk)

Received 24 July 2024; Accepted 19 September 2024

Academic Editor: Jing Shi

Copyright © 2024 Feras Alasali et al. This is an open access article distributed under the Creative Commons Attribution License, which permits unrestricted use, distribution, and reproduction in any medium, provided the original work is properly cited.

The increasing use of inverter-based distributed generation requires a comprehensive study of its effects on fault analysis and the effectiveness of protection systems in distribution networks. This study examines the impact of different inverter control modes on multiple types of protective relay schemes. These include different overcurrent relay (OCR) schemes, both standard and nonstandard tripping characteristics, optimal coordination approaches, and different grid operation scenarios. The investigation is conducted through the utilization of grid-connected and islanding operation modes, with fault resistance values of 0 and 5  $\Omega$ . The study is carried out on a 14-bus CIGRE network which includes two photovoltaic (PV) farms with a capacity of 10 MVA each. The research provides several significant contributions, including the analysis of fault current contributions, examination of issues in OCR protection, investigation of the influence of fault impedance levels on OCR performance, evaluation of ideal coordination methods, and carrying out a comparative analysis utilizing optimization technique by using the water cycle optimization algorithm (WCA) and the particle swarm optimization algorithm (PSO). In addition, to guarantee the robustness of the suggested protection strategy, this work adopts a hardware-in-the-loop approach. The OMICRON-256 system is utilized to carry out real-time testing on a SIPROTEC 7SJ62 multifunction protection relay, which validates the effectiveness of the proposed method in protecting microgrids under different PV control strategies. The total operating time for the nonstandard tripping scheme was 12.077–12.3003 s for PSO and WCA, respectively, while for the standard tripping scheme, it was 12.1226 and 12.1564 s. Moreover, these findings offer practical insights that can assist operators in effectively designing the power networks with grid-connected PV systems by showing OCR miscoordination and no tripping events in power systems with PVs under inverters controllers.

**Keywords:** distribution generation; optimal coordination; overcurrent relays; PV controllers

## 1. Introduction

*1.1. Motivation.* In recent years, the power system has been undergoing a gradual transition from the conventional system dominated by synchronous generators (SGs) to a highly interconnected system with a significant presence of photovoltaic

(PV) sources. To mitigate the power fluctuations caused by the intermittent nature of PV sources, these sources are integrated with the grid through inverters [1]. To ensure the reliability of the interconnected inverter-based distributed generation (IIDG), many countries have implemented grid codes that take into account the thermal capabilities of semiconductor

switches. These grid codes incorporate requirements such as fault ride-through (FRT) capabilities at both low and high frequencies [2] to limit the fault current. However, the fault current characteristics can be influenced by different control techniques employed by IIDG [3]. It has been reported in the literature that the fault current,  $I_f$ , contributed by IIDG is generally within the range of 1.1–2 times the rated current,  $I_R$  [3, 4]. This low fault current magnitude makes it challenging to detect faults using conventional overcurrent relay (OCR) in distribution systems [2, 4]. Moreover, the fault current level depends on factors such as real-time power generation capacity and the location of PV sources [5]. The cumulative effect of these factors can lead to relay misoperation, compromising the security of the system, as well as loss of relay coordination and relay blinding, causing dependability issues. Therefore, it is vital to address the influence of the evolving distribution power system on fault detection and protection. This necessitates the investigation of the impact of different control techniques employed by IIDG on identifying faults, developing a sensitive power protection system, and ensuring the robustness and stability of the power grid during its transition to a more sustainable and renewable energy-based system. This paper attempts to be one of the first to investigate the challenges of OCR protection proposals and coordination associated with defect detection in the context of the changing dynamics of power systems under different control techniques on PV inverters.

*1.2. Literature Review.* PV-connected systems have a significant impact on the short-circuit current in power systems, thereby influencing their overall short-circuit capacity [6, 7]. In different studies, the individual contribution of a single PV system to the fault current is negligible due to its small size and the current limitations of the inverter, a high penetration of PV systems in the power networks can substantially alter the fault currents, leading to adverse effects on the protection system's operation [3, 8]. Therefore, it is crucial to model the contribution of PV systems to the fault current and extend the traditional short-circuit analysis to accommodate power networks with PV system integration. The short-circuit analysis serves various purposes, such as evaluating fault current magnitudes to determine the breaking capacity of interrupting devices and establishing a basis for protection system coordination such as OCR to ensure selectivity. Several factors influence the contribution to the short-circuit current, including environmental conditions, maximum inverter current flow, self-protections of PV systems, fault location and type, and the behavior of the PV system during faults, primarily governed by the inverter control system [9, 10]. The short-circuit current computation (SCC) plays a crucial role in relay protection settings and coordination, fault location, and supply restoration. SCC results are also essential for selecting protection equipment and designing busbars, ensuring overall system safety and differentiation. Consequently, real-time SCC must have two essential qualities: speed and high accuracy [11]. However, during faults, the behavior of IIDGs differs significantly based on internal logic control. The SCC contribution of IIDGs is typically

within the range of 1.06–1.2 p.u. on the base rating [8, 12–14], or 1.1–1.5 p.u. according to other studies [15, 16]. Furthermore, the SCC waveform exhibits a fast initial spike lasting a few 100  $\mu$ s or less, potentially exceeding 2.0 p.u. on the IIDG's base rating, followed by a regulation period of a few 100 ms, which varies based on technology and manufacturer control [17].

In addition, IIDGs operate as grid-following devices, independent of the distribution grid operator (DGO) or consumer unit, and are commonly associated with variable renewable energy sources, such as PV [18, 19]. For example, the control strategy employed by IIDGs significantly influences the characteristics of the fault current, particularly when considering the low voltage ride-through (LVRT) control strategy. The LVRT requirements necessitate the adjustment of IIDG control strategies, including constant power, FRT, and off-grid modes [20, 21]. Previously, the contributions of inverter-based distributed generators (IIDGs) to fault currents were typically disregarded in steady-state fault calculations due to their limited magnitude, usually within 50% of the rated current of the inverter [22–24]. However, modern grid code standards increasingly require IIDGs to remain connected during faults to support grid voltages by injecting positive-sequence reactive current and aid in fault recovery through reactive power injection [25–27]. This is particularly significant in microgrid applications where IIDGs may serve as the primary energy source. With the implementation of grid code standards, such as LVRT and reactive current injection (RCI) requirements, as well as the growing integration of IIDGs in power systems, the fault current contributions from IIDGs can no longer be neglected. Furthermore, advanced grid code requirements for microgrid operation may mandate IIDGs to inject negative sequence current as well, serving as a fault detection signal for microgrid controllers [28–30]. Accurate modeling of IIDGs for fault current calculations is crucial for applications such as adaptive and new relay protection schemes [31, 32]. However, the widely adopted IEC 60909 standard for fault calculations has not been updated to adequately consider these essential aspects of IIDGs, initially neglecting their contributions to fault currents [24]. The most recent revision of the standard [33] acknowledges the fault current magnitude but overlooks the active and reactive components that rely on voltage dip and specific LVRT and RCI requirements. Nevertheless, in cases where faults occur near the IIDG's connection point with significant voltage dips, the IIDG's fault current consists primarily of reactive components, rendering the standard models inaccurate. Inaccurate IIDG models derived from the IEC 60909 standard can lead to flawed fault calculation results, particularly concerning fault current distribution, thereby compromising the appropriate configuration of relay settings and coordination. This issue is particularly critical in microgrids with high IIDG penetration, especially during islanded operation [34], where IIDGs serve as the primary source of power generation.

As smart inverter-based distributed energy resources become more important, automation and system integration are increasingly crucial for real-time monitoring of key variables at both distribution substations. These real-time data enable

distribution system operators to respond to ensure the reliable and continuous operation of smart inverters while coordinating with transmission system operators during steady-state, dynamic, and transient events [35]. The study [35] has reported that faults have led to the loss of a substantial amount of PV generation. These incidents were recorded by a supervisory control and data acquisition system, which operates at a sampling rate of one sample every 4 s. Improved visibility would enhance the understanding of distributed energy resource responses across local electrical power systems, and even wider networks. Additionally, the growing presence of smart inverters in the distribution network (DN) is replacing a significant share of the reactive power resources traditionally connected to the transmission network. However, with the high penetration of distribution generations (DGs), the system dynamics and interdependence between the distribution and transmission networks have strengthened, making it necessary to treat them as interconnected systems. This growing interconnection means DNs now play a more active role in supporting transmission network operations during both normal and abnormal conditions [36]. This highlights the importance of studying and investigating the impact of PV systems and inverter control models on the power system and short-circuit calculations.

*1.2.1. The Short-Circuit Calculation Standards in the Presence of Renewable Energy Resources.* The IEC standards and software simulations before 2003, used for fault calculations did not take into account the significant contributions of software IIDGs to fault currents. As shown in Table 1, which references [37–55], the gap in the research is highlighted. The short-circuit calculations in [37–39, 56] conducted in 2000 and 2001 were based on IEC 60909, disregarding the contributions of IIDGs, as well as inverter limits and grid support. Furthermore, enhancements to the procedures were made in [40, 41] in 2011; however, they did not account for the contribution of IIDGs to fault current. In [42, 43] studies, published in 2016, IIDG presence and its contribution to fault current were considered using calculations based on IEC 60909-2016, without the use of additional software. By IEEE 1547-2018 [44], assumed that all factors related to IIDG would be concealed during short-circuit calculations when an IIDG is present. The inclusion of IIDG in the DIgSILENT PowerFactory software was introduced in 2019 [45]. In Li and Wang's [47] and Kim's [48] studies, calculations were performed using MATLAB software and based on the IEEE standards. A new standard, IEEE 2800, was developed in [52] for 2022, considering IIDG's contribution to fault current, inverter limits, and grid support. To further enhance their results, Mabote et al. [50] and Davi et al. [51] utilized PowerModels and PSCAD/EMTDC based on IEEE 2800-2022. Subsequently, in 2023, the IIDG's short-circuit contribution was incorporated into the ETAP program [54]. Table 1 highlights substantial progress in inverter control during fault scenarios. While there is a growing emphasis on this area of research to enhance grid support, traditional overcurrent protection devices have been remained underdeveloped. These conventional devices face challenges

in detecting or isolating faults because the fault current differs based on the type of smart inverter control. Furthermore, traditional protection systems were designed for fault currents from conventional grids, but with the introduction of solar energy, both the magnitude and direction of fault currents have changed significantly.

*1.3. Contributions.* The protection system for a DN with IIDG encounters numerous challenges. Inverter control plays a crucial role in the control strategy during faults, as dictated by IEEE 1547 and grid code specifications. The fault characteristics differ between distribution systems with and without renewable energy sources, which adds complexity to conventional protection schemes. The previous section presents the recent literature review on investigating the impact of inverter control model during faults. Through the literature review, significant advancements in inverter control during fault occurrences are observed. In cases of faults, it is imperative to isolate the fault and protect equipment using overcurrent protection devices, whether conventional or nonconventional. In this work, the contribution of fault current from different PV systems and under five different control strategies of IIDG is investigated. This investigation highlights the significant impact of control strategies and fault locations on the fault current contributions of IIDG systems. Then, this paper aims to provide an early exploration of the challenges related to defect detection and coordination of OCR protection schemes in the context of evolving power systems, specifically focusing on the influence of different control techniques employed in PV inverters. The results indicate that certain types of control methods increase the challenges for current protection devices in fault detection, and in some cases, they trip with a delay, which increase risks to the grid. As the dynamics of power systems change, it becomes crucial to examine the implications for OCR protection and coordination. By addressing this research gap, the paper seeks to contribute to the understanding of OCR protection in the context of evolving power systems and the impact of various control techniques used in PV inverters. The contributions of this paper are outlined as follows:

- Investigating the contribution of fault current from different PV systems under five PV control strategies employed by IIDGs. By analyzing the impact of control strategies and fault locations on fault current contributions, the study highlights the significance of these factors in understanding the behavior of IIDG systems during faults at a 14-bus CIGRE network with two 10 MVA PV farms.
- Early exploration of challenges in OCR protection: The paper addresses the research gap by conducting an early exploration of the challenges associated with defect detection and coordination of OCR protection schemes in evolving power systems. Specifically, the focus is on examining the influence of different control techniques utilized in PV inverters. This investigation contributes to the understanding of OCR protection within the context of evolving power systems and light

TABLE 1: Summary short-circuit calculation standards in the presence of renewable energy resources.

Ref. no.	Short-circuit calculation model		IIDG contributions to the fault current	Inverter limits	Voltage support (grid code)
	Standards	Software			
38	2000	IEEE 929-2000	X	X	X
39	2001	IEC 60909-2001	X	X	X
40	2001	IEEE 242-2001	X	X	X
41	2003	IEEE 1547-2003	X	X	X
42	2006	X	✓	X	X
		MATLAB			
43	2011	IEEE 1547.2011	✓	X	X
44	2016	IEC 60909-2016	✓	X	X
45	2018	IEEE 3002.3-2018	X	X	X
46	2018	IEEE 1547-2018	✓	✓	✓
47	2019	IEC 60909	✓	✓	✓
48	2021	IEC 60909-2021	✓	✓	✓
49	2021	X	✓	✓	✓
		DigSILENT PowerFactory			
50	2021	IEEE 1547-2018	✓	✓	✓
51	2022	IEEE 2800	✓	✓	✓
		X	✓	✓	✓
52	2023	IEEE 2800-2022	✓	✓	✓
53	2023	X	✓	✓	✓
		PowerModels.jl (PMs)			
54	2023	X	✓	✓	✓
		PSCAD/EMTDC			
55	2023	IEEE 2800-2022	✓	✓	✓
		X	✓	✓	✓
		MATLAB			
56	2023	IEEE 1547-2018	✓	✓	✓
		IEC 60909-2021	✓	✓	✓
		ETAP			





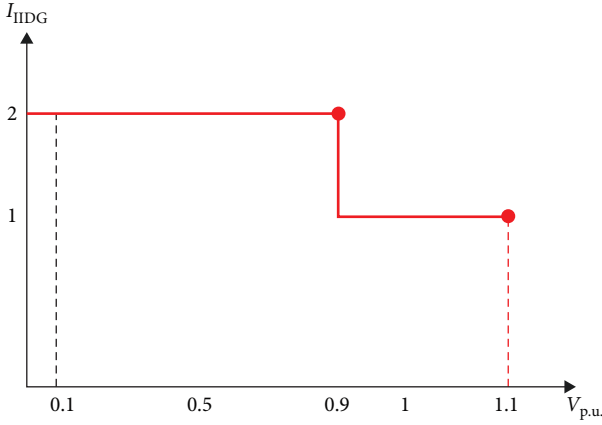


FIGURE 2: Control strategy A.

currents being smaller than healthy phase currents. This complicates the identification of the faulty phase based on the phase's current magnitude. In the subsequent section, the impact of various operating modes (five main IIDG control categories) on the contribution of fault current by a PV plant is described and presented.

**2.1. Control Strategy A.** The control strategy, mode A, described by Equation (2) imposes a limitation of 2.0 p.u. on the controlled fault current, determined by the PCC voltage,  $V_{PCC}^+$ . Figure 2 demonstrates the relationship between the current supplied by the IIDG ( $I_{IIDG}$ ) and  $V_{PCC}^+$ . Specifically, if the bus voltage falls within the range of 0.9–1.1 p.u., the current is reduced to 1.0 p.u. This control characteristic ensures that the fault current remains within specified limits based on the PCC voltage:

$$I_{IIDG} = \begin{cases} 2 & 0 \leq |V_{PCC}^+| \leq 0.9 \\ 1 & 0.9 < |V_{PCC}^+| \leq 1.1 \end{cases} \quad (2)$$

**2.2. Control Strategy B.** Following the guidelines outlined in the German grid code [55, 57], it is mandatory for PQ for DGs, including turbine generations and PVs, within a microgrid to possess the LVRT capability. This feature enables these DGs to support voltage levels during fault conditions by injecting reactive power. The fault current,  $I_{IIDG}$ , as depicted in Figure 3 and determined by Equations (3), is categorized into three distinct areas based on the  $V_{PCC}^+$  level. These divisions allow for a better understanding of the fault current behavior and assess the impact of the LVRT capability on voltage stability within the microgrid. This control characteristic implemented for fault current regulation ensures that if the  $V_{PCC}^+$  falls between 1 and 1.1 p.u., the current is limited to 1 p.u. In case, the  $V_{PCC}^+$  recorded level under 0.5 to 0 p.u., the  $I_{IIDG}$  is limited to 2 p.u. In addition, this control strategy effectively maintains the fault current when  $0.5 < |V_{PCC}^+| \leq 1$  by using a linear limits relationship between the voltage and current level at the PCC ( $I_{IIDG} =$

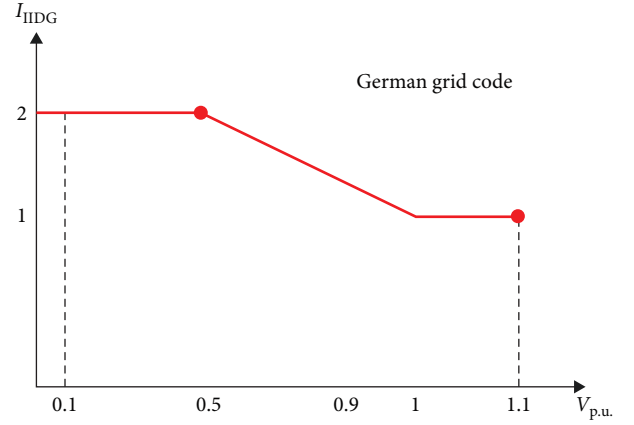


FIGURE 3: Control strategy B based on the German grid.

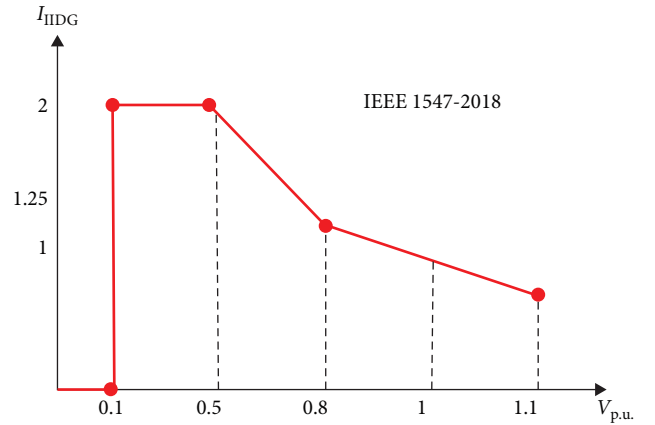


FIGURE 4: Control strategy C based on the IEEE 1547-2018.

$-2.5 \cdot |V_{PCC}^+| + 3.25$ ) for ensuring the stability and reliability of the system:

$$I_{IIDG} = \begin{cases} 2 & 0 \leq |V_{PCC}^+| \leq 0.5 \\ -2.5 \cdot |V_{PCC}^+| + 3.25 & 0.5 < |V_{PCC}^+| \leq 1 \\ 1 & 1 < |V_{PCC}^+| \leq 1.1 \end{cases} \quad (3)$$

**2.3. Control Strategy C.** As per the guidelines specified in IEEE 1547-2018 [10, 55], IIDGs are required to withstand fluctuations in voltage while facilitating the exchange of active and reactive power with the grid. Therefore, it is required to support multiple operational modes such as Volt–Watt, Volt–VAR, Watt/VAR, constant power factor, and constant reactive power. The control strategy, mode C, is employed to enable the flow of fault current through different stages. The  $I_{IIDG}$  is limited under five areas, as described in Equation (4) and shown in Figure 4. This flexibility in controlling the fault current,  $I_{IIDG}$ , behavior allows for effective adaptation and optimization of the IIDG's response to various grid conditions, enhancing the overall stability and performance of the system:

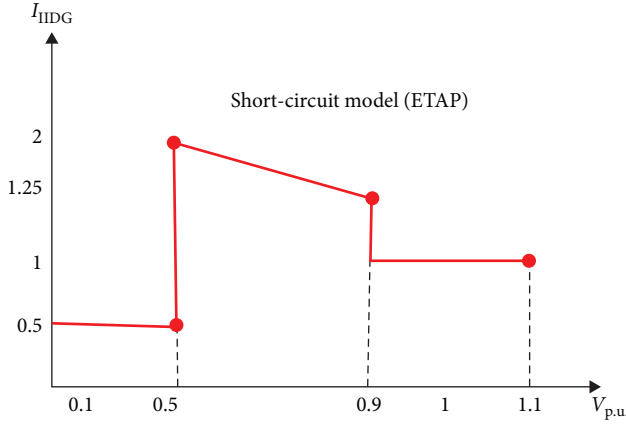


FIGURE 5: Control strategy D based on the IEEE 1547 standard, ETAP.

$$I_{IIDG} = \begin{cases} 0 & 0 \leq |V_{PCC}^+| \leq 0.1 \\ 2 & 0.1 < |V_{PCC}^+| \leq 0.5 \\ -2.5 \cdot |V_{PCC}^+| + 3.25 & 0.5 < |V_{PCC}^+| \leq 0.8 \\ 1 \cdot |V_{PCC}^+| + 2 & 0.8 < |V_{PCC}^+| \leq 1 \\ -1 \cdot |V_{PCC}^+| + 2 & 1 < |V_{PCC}^+| \leq 1.1 \end{cases} \quad (4)$$

**2.4. Control Strategy D.** The current-limiting effect and operational modes of the inverter, as specified by the equations in the IEEE 1547 standard, were analyzed using the transient analysis software ETAP. The behavior of the inverter during fault conditions, generation mode, and shutdown was visually represented on the inverter SC model page, providing a comprehensive understanding of its response. This study employed a combination of numerical simulations and graphical illustrations to investigate the current-limiting capabilities and diverse operating scenarios of the inverter, aligning with the requirements outlined in the IEEE 1547 standard, as described in Equation (5) and shown in Figure 5:

$$I_{IIDG} = \begin{cases} 0.5 & 0 \leq |V_{PCC}^+| \leq 0.5 \\ -2.5 \cdot |V_{PCC}^+| + 3.25 & 0.5 < |V_{PCC}^+| \leq 0.9 \\ 1 & 0.9 < |V_{PCC}^+| \leq 1.1 \end{cases} \quad (5)$$

**2.5. Control Strategy E.** In the IEEE 1547 standard and ETAP [10, 55], the presented control strategy, mode E, is more flexible compared to mode D, as shown in Figure 6. The control mode E is implemented based on three areas for fault current regulation. First, if the  $V_{PCC}^+$  falls between 0.9 and 1.1 p.u., the current is limited to 1 p.u. In case, the  $V_{PCC}^+$  the recorded level between 0.5 to 0.9 p.u., the  $I_{IIDG}$  is limited based on the linear limits relationship between the voltage and current level ( $I_{IIDG} = -2.5 \cdot |V_{PCC}^+| + 3.25$ ). In addition, this control strategy effectively maintains the fault current

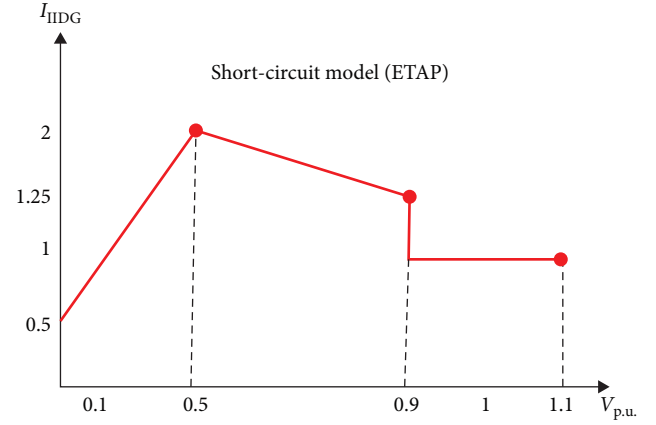


FIGURE 6: Control strategy E based on the IEEE 1547 standard, ETAP.

when  $0 \leq |V_{PCC}^+| \leq 0.5$  by using a linear limits relationship between the voltage and current level at the PCC ( $I_{IIDG} = 3|V_{PCC}^+| + 0.5$ ):

$$I_{IIDG} = \begin{cases} 3|V_{PCC}^+| + 0.5 & 0 \leq |V_{PCC}^+| \leq 0.5 \\ -2.5 \cdot |V_{PCC}^+| + 3.25 & 0.5 < |V_{PCC}^+| \leq 0.9 \\ 1 & 0.9 < |V_{PCC}^+| \leq 1.1 \end{cases} \quad (6)$$

### 3. Problem Statement: OCRs Coordination for Power Network With IIDGs

The OCR protection scheme for a power network equipped with IIDGs encounters various challenges, especially during fault conditions. As previously discussed, inverter control plays a crucial role in the control strategy, as emphasized by IEEE 1547 and grid code specifications. Figure 7 illustrates the power distribution system that receives power from the main grid and IIDGs, which is then distributed through lines and protected using OCRs. In the absence of PV1 and PV2, if a fault occurs at point F1, the fault current contribution is only from the main grid, and primary protection operation by R1 is necessary to safeguard the line. In case of R1 delay or failure to detect the fault, R2 acts as a backup with coordination time interval (CTI) considerations between the two relays. However, when PV1 and PV2 are connected to the grid, the fault current contribution involves the main grid as well as PV1 and PV2, and the magnitude of the fault current depends on the control strategy employed by PV1 and PV2. First, when both inverters 1 and 2 operate under control strategy A, the fault current contribution from PV1 and PV2 is twice their full-rated current. R1 and R4 act as primary protection relays, detecting and isolating the fault, while R2 serves as a backup. However, in compliance with IEEE 1547-2018 and IEEE 2008-2022, inverters must support the grid and consider its requirements and limitations. Second, advanced control strategies (B, C, D, and E) are now



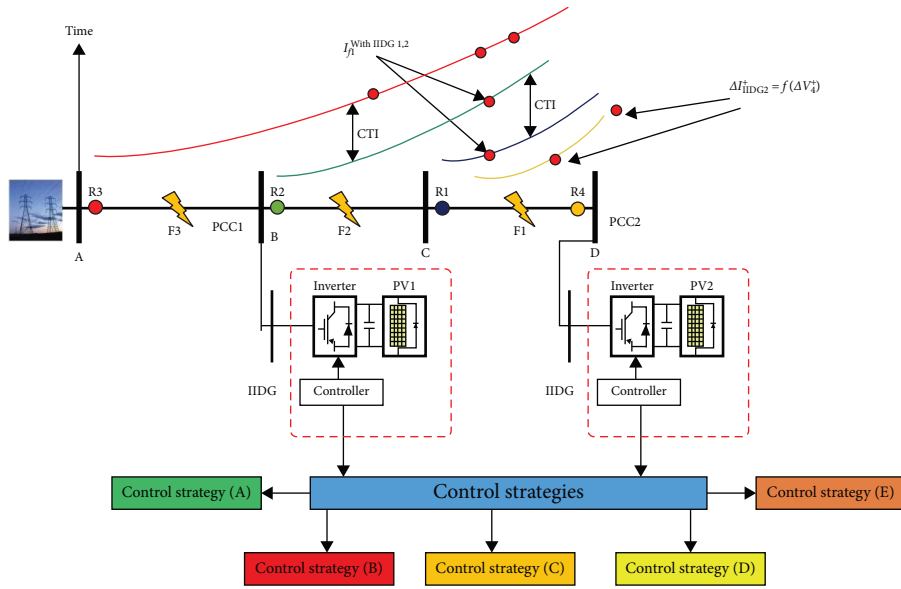


FIGURE 7: Single line diagram of the power network equipped with DG and three fault scenarios.

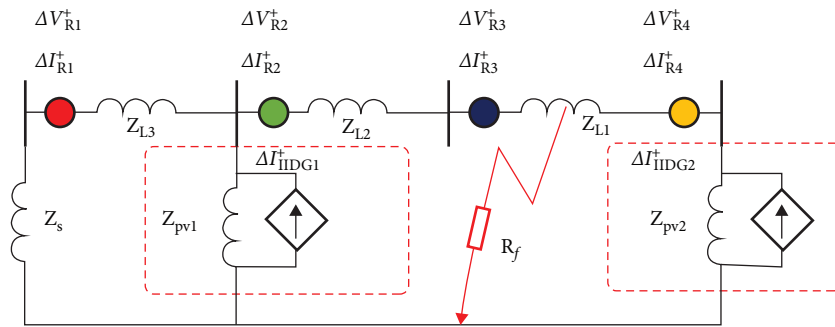


FIGURE 8: A positive-sequence network of the distribution network when an internal fault occurs at point F1.

widely employed in practical applications and research, and they are also integrated into electromagnetic transient programs. The fault characteristics differ between distribution systems with different control strategies, causing challenges to conventional protection schemes.

The control strategy employed by the IIDG significantly influences its output current and the behavior of its output current. However, the implementation of a positive-sequence control strategy in IIDG offers benefits such as enhanced stability and simplified control system architecture. By adopting this strategy, the IIDG focuses solely on providing positive-sequence current, streamlining its operation, and ensuring a more stable performance. During its current-limiting modes, as described in Section 2, the inverter is designed to inject a consistent current into the network, adhering to the maximum limit set by the current-limiting curve. Consequently, it can be viewed as a constant-current source in relation to its current magnitude, although not in terms of its active and reactive components. The distribution of the inverter current's active and reactive components is dictated by one of three operating modes: reactive current priority, real power priority, or user-defined power factor. These modes determine the

prioritization and control of the inverter's active power and reactive power contributions. Therefore, it is vital to investigate the influence of the evolving control strategies on fault detection and OCR protection schemes. Figure 7 shows the impact of the fault component's voltage ( $\Delta V^+$ ) and current ( $\Delta I_{IIDG}^+$ ) on the OCR schemes for OCRs (R1–R4). The fault components,  $\Delta V^+$  and  $\Delta I_{IIDG}^+$ , are described as the difference between the prefault and postfault voltages and current, respectively. As shown in Figure 7, when control strategy B is implemented in PV1 and PV2 and a fault occurs (F1) at 30% of line 3 (L3), PV1 contributes approximately twice its rated current, while PV2's contribution is less than 1.4 times its rated current. The variation in fault contributions between IIDGs and the low current levels observed across different voltage regions, as depicted by Equations (3)–(6), directly influences the performance of OCRs in terms of their selectivity and sensitivity.

Figure 8 provides a clearer representation of the positive network during fault case F1. The line impedance is represented by  $Z_L$ , and  $Z_s$  denotes the equivalent impedance of the power supply. The  $I_{F1}^+$  represents the fault current at the fault point (F1), while  $\Delta I_{IIDG1}^+$  and  $\Delta I_{IIDG2}^+$  represent the fault

current components contributions of the IIDG at PV1 and PV2 to the fault point. The fault current magnitude  $\Delta I_{IIDG1}^+$  and  $\Delta I_{IIDG2}^+$  are determined by multiple factors, including the intermittent nature of renewable energy sources, variations in positive-sequence voltage  $\Delta V_{R2}^+$  and  $\Delta V_{R4}^+$ , respectively, by the control function  $f$ . By applying Kirchhoff's current law and considering Equations (7)–(12), it becomes evident that the fault current contributed by IIDG directly impacted the fault characteristics, where  $\Delta I_{R1}^+$ ,  $\Delta I_{R2}^+$ ,  $\Delta I_{R3}^+$ , and  $\Delta I_{R4}^+$  are the fault current components at OCR1–4, respectively, while  $R_f$  is the fault resistance:

$$I_{F1}^+ = \Delta I_{R3}^+ + \Delta I_{R4}^+, \quad (7)$$

$$\Delta I_{R4}^+ = \Delta I_{IIDG2}^+, \quad (8)$$

$$\Delta I_{R2}^+ = \Delta I_{R1}^+ + \Delta I_{IIDG1}^+, \quad (9)$$

$$\Delta I_{R3}^+ = \Delta I_{R2}^+, \quad (10)$$

$$\Delta I_{IIDG1}^+ = f(\Delta V_{R2}^+), \quad (11)$$

$$\Delta I_{IIDG2}^+ = f(\Delta V_{R4}^+). \quad (12)$$

**3.1. The Problem Formulation of Optimum OCRs Coordination.** Recently, the coordination problem of OCRs in a distribution power network with PV systems (IIDGs) has been addressed as an optimization problem. The main objective of this optimization is to determine optimal OCR settings that minimize the overall operational time of OCRs while maintaining the selectivity between primary and backup relays. In this section, the mathematical formulation of our proposed optimization approach is presented, which aims to solve the coordination problem and enhance the performance of OCR optimization strategies. To achieve this, an objective function (OT) is introduced to minimize the total operating time of primary and backup OCRs. The mathematical expression for the objective function is given by Equation (13) and described in detail in [59]:

$$OT = \sum_{r=1}^R \sum_{f=1}^F t_{r,f}. \quad (13)$$

The operational time of a relay, denoted as  $t_{r,f}$ , plays a crucial role in the OCRs within a DN. In this context,  $t_{r,f}$  represents the time taken by relay  $r$  to operate when a fault occurs at location  $f$ . The total number of OCRs in the DN is denoted by  $R$ , and  $F$  represents the total number of fault locations within the network. By considering these variables, we can accurately assess the performance and efficiency of the OCR coordination strategy in terms of relay operational times at different fault locations throughout the DN. The formulation of OT is guided by a set of constraints that must be satisfied. These constraints serve as limitations or conditions imposed on the optimization problem. The fulfillment of these constraints ensures the feasibility and validity of the optimization solution:

- Selectivity constraints:

$$t_{\text{backup}} - t_{\text{primary}} \geq \text{CTI}. \quad (14)$$

The operational time for both the primary and backup OCRs, denoted as  $t_{\text{primary}}$  and  $t_{\text{backup}}$ , respectively, plays a crucial role in achieving selectivity and efficient performance. The value of the CTI, as described in Equation (14), is a determining factor for these operational times and depends on various criteria such as the relay type and circuit breaker speed. To ensure selectivity, the CTI is typically set within the range of 0.2–0.5 s, as recommended by the IEEE-242 standard. In this study, we adopt a CTI value of 0.3 s, which aligns with previous research [59, 60]. The CTI value serves as an essential parameter in the optimization process, enabling the establishment of appropriate operational times for the primary and backup OCRs while maintaining selectivity.

- Relay settings constraints:

$$t_{\min} \leq t_r \leq t_{\max}, \quad (15)$$

$$\text{TMS}_{\min} \leq \text{TMS}_r \leq \text{TMS}_{\max}. \quad (16)$$

The constraints for the optimization problem include the minimum and maximum operational times ( $t_{\min}$  and  $t_{\max}$ ) for the OCRs, as shown in Equation (15), where  $t_r$  represents the operational time of relay  $r$ . The time multiplier setting (TMS) also imposes constraints, as presented in Equation (16), with  $\text{TMS}_{\min}$  and  $\text{TMS}_{\max}$  representing the minimum and maximum values, respectively. Each relay  $r$  has its assigned TMS value ( $\text{TMS}_r$ ). In this study, the TMS is treated as a continuous variable, and the OCRs must operate within the prescribed protection scheme's time limits. Thus, the TMS needs to be set within the allowable range for various fault conditions and even during light overloads. The TMS limits typically span from 0.01 to 3 [60], encompassing the majority of industrial and microgrid OCRs.

**3.1.1. Current–Time Characteristics for OCRs.** The operational time,  $t_r$ , of OCR, as presented in Equation (13), is typically determined using a standard inverse function relating to the fault current and operational time [60–63]. The specific characteristic equation governing the relay's response varies depending on the manufacturer and type of OCR utilized, as detailed in [59]. In this study, we adopted and employed two current–time characteristics, standard and detailed nonstandard OCR characteristics, to investigate the impact of IIDGS on OCRs performance.

- Standard OCRs characteristic: The IEC255-3 standard characteristic equation, represented by Equation (17), as a reference and common scheme [59, 60]:

$$t_r = \left[ \frac{A}{\left(\frac{I_r}{I_p}\right)^B - 1} \right] \text{TMS}. \quad (17)$$

Equation (17) represents the inverse time characteristic of the OCR, where  $I_f$  denotes the fault current,  $I_p$  represents the pickup current and constants A and B are determined based on established OCR standards such as IEEE and IEC. Numerical and programable relays, including microprocessor-based OCRs, offer the flexibility to adjust their time-operating properties through network connections and real-time data updates. In this research, numerical OCRs adhering to the industry-standard IEC specifications are utilized, with A and B values set at 0.14 and 0.02, respectively [59, 60].

- Nonstandard OCR characteristics: The nonstandard time–current characteristic equation, represented by Equation (18), as an advanced and new scheme compared to inverse standard characteristic. The proposed nonstandard OCR characteristics incorporate a logarithmic function [57] as their fundamental element:

$$t_r = \left( 5.8 - 1.35 \times \log_e \left( \frac{I_f}{I_p} \right) \right) \text{TMS.} \quad (18)$$

The primary objective of using nonstandard OCR characteristics is to minimize the tripping time associated with different fault currents. The performance of the proposed nonstandard characteristic scheme will be compared to the standard OCR scheme, specifically the inverse definite minimum time characteristic [61]. The applicability of the nonstandard OCR characteristics extends beyond OCR coordination and can be useful in addressing thermal stress concerns in equipment such as transformers and cables.

**3.1.2. Optimization Algorithms.** In this section, the coordination problem of OCRs in a DN equipped with PVs is formulated as an optimization task with specific constraints. To solve this coordination problem and minimize the tripping time of OCRs, the WCA and PSO have demonstrated effectiveness in solving complex power network and protection problems. The choice of these two optimization algorithms is based on their reputation as powerful and effective methods for tackling complex problems in engineering. Extensive research has shown that these algorithms have the capability to address intricate engineering challenges and deliver promising results. They have demonstrated their effectiveness in various applications and are well-regarded for their ability to handle complex optimization tasks. Their selection for this study is driven by their proven track record in solving intricate engineering problems, providing confidence in their potential to tackle the specific optimization challenges at hand.

The WCA draws inspiration from the natural water cycle and has been found to outperform standard optimization algorithms. The optimization process is implemented using the MATLAB/SIMULINK toolbox. The application of the WCA approach for microgrid protection coordination is described in previous works [62]. In our study, the WCA is utilized to achieve the minimum tripping time for all OCRs (primary and backup) by solving Equation (13) while considering the relay constraints presented in Equations (14)–(16). On the other hand, PSO is a contemporary and efficient

heuristic optimization method that offers computational efficiency and memory conservation due to its inherent simplicity. It draws inspiration from human social behavior and the swarming behavior of animals. The fundamental principle of PSO involves managing and guiding a population of particles (referred to as a swarm), with each particle representing a potential solution. By utilizing the collective intelligence of the swarm, PSO aims to find optimal solutions to complex problems. The swarm population in PSO serves as the solution space, and individual particles within the swarm represent potential solutions that undergo iterative improvements throughout the optimization process [63].

#### 4. Simulation Results and Discussion

In the results section, the evaluation of the OCR protection schemes for the PV inverters contribution problem in the power network discussed in Sections 2 and 3 is presented. The assessment is conducted using a 14-bus DN based on the CIGRE network model. The objective of this study is to test and evaluate the effectiveness of the proposed OCR scheme under different modes of DN operation, including islanding mode. Furthermore, the investigation in this section focused on examining the fault current contribution of incorporated two 10 MVA PV farms operating under five distinct control strategies employed by IIDGs. The findings contribute to a deeper understanding of fault current dynamics in IIDG systems, offering valuable guidance for the development of effective fault management strategies and enhancing the overall stability and reliability of the OCR protection system in the DNs. In addition, a comparison is made between the proposed scheme utilizing nonstandard and standard tripping curves. The evaluation provides valuable insights into the performance and superiority of the proposed OCR scheme in various operational PV scenarios, highlighting its potential challenges over traditional protection methodologies. Then, the impact of different levels of fault impedance on OCR performance under various PV control models and penetration scenarios is discussed. A comparative analysis of the proposed optimal OCR coordination approaches is performed under different fault, and PV operation scenarios by using the WCA and the PSO are shown. Finally, the HIL testing results are presented.

**4.1. Description of the DN.** The proposed CIGRE network utilized in this study is a 14-bus DN with specific details provided in [64]. It operates with a high-voltage/medium-voltage (HV/MV) utility source and incorporates two 10 MW PV farms connected through a set-up transformer with a rating of 0.4/12.49 kV, as outlined in [64]. Each 10 MW farm consists of 10 1 MW PV systems. The CIGRE network is protected by a total of 12 OCRs, with primary and backup OCRs assigned to each of the 12 fault locations labeled from F1 to F12. These fault locations represent near- and far-end locations from the sources to evaluate the impact and contribution of the different PV operating control scenarios on the fault detection and protection schemes. The details of the OCRs at the CIGRE network are presented in Table 2 and depicted in Figure 9. To ensure accurate performance, initial

TABLE 2: The fundamental parameters of the CIGRE network's OCRs.

OCR	CT ratio	Pickup current (A)
OCR1–4	200/1	50
OCR5 and OCR6	200/1	150
OCR7–12	200/1	50
OCR13 and OCR14	300/1	300

load flow and fault calculations were conducted to determine the current transformer ratio and pickup current for each OCR, adhering to the IEC 60909 standard. In this study, the TMS for each OCR is calculated optimally based on the maximum load currents in the line and various fault scenarios, including LLL faults. To ensure the prompt operation of the primary OCRs, the CTI is selected to be 0.3 s [57]. Additionally, the pickup current for the OCRs is set at 1.2 times the full load current. These parameter settings are crucial in achieving fast and reliable operation of the OCRs, taking into account the load characteristics and fault scenarios.

**4.2. Simulation Results.** With the growing integration of renewable energies into the grid, managing both active and reactive power during faults has become crucial. Several control methods, as shown in Table 1, have been proposed to enhance the flexibility of the grid. This study focuses on the most common types of control methods, Control A, B, C, D, and E including those used in the Germany grid code and IEEE 1547:2018, as well as other methods currently in use. The primary goal is to assess how various inverter control methods affect fault contributions and the performance of OCR protection schemes across different DN operation models. In this results section, the performance of the fault contributions characteristics and the performance of the OCR protection scheme under varies inverter control modes are evaluated across different DN operation models. In addition, the focus is on investigating the impact of the PV control model on the modern OCR coordinating scheme (standard and nonstandard), which utilizes modern optimization methods and algorithms, under different grid configurations. The results provide valuable insights into the performance comparison between the OCR schemes under various fault scenarios. This evaluation enables a comprehensive understanding of the effectiveness of the OCR schemes in different grid and PV control configurations. The CIGRE network operation modes:

- *Scenario A:* The power sources of the CIGRE network consist of a main HV/MV utility feeder and two 10 MVA PV farms, as illustrated in Figure 9. The objective of this grid operation is to assess the performance and power grid and the OCR scheme in the presence of utility supply and under different PV control modes. As explained in Sections 2 and 3, the introduction of PVs introduces complexities in changing the fault contributions characteristics and achieving optimal coordination of OCRs. In addition, by studying the grid performance under different levels of fault impedance (0 and 5  $\Omega$ ),

this evaluation of the CIGRE network aims to provide valuable insights into the challenges for achieving optimal OCR coordination in modern power network configurations with PV integration.

- *Scenario B:* In islanding mode, a specific section of the DN remains energized by only the PV systems, even in the presence of internal faults. By operating the CIGRE network in islanding mode and evaluating the performance of the OCR scheme and fault contributions characteristics across different levels of fault impedance (0 and 5  $\Omega$ ), the research highlights the challenges of developing OCR protection schemes and maintaining power supply during fault conditions and enhancing the stability of the grid in case of islanding mode.

The following detailed testing procedure aims to provide a thorough understanding of how various inverter control methods influence the performance of OCR protection schemes and the overall stability of modern power grids with integrated renewable energy sources:

- **Network configuration:** Setup the CIGRE network, as shown in Figure 9, according to the configurations for Scenarios A and B.
- **Inverter control methods:** Implement the five control methods (Control A, B, C, D, and E) in the network. These methods include those outlined in the Germany grid code and IEEE 1547:2018, as well as other prevalent control approaches.
- **Fault injection:** Simulate fault conditions with varying impedances (0 and 5  $\Omega$ ) to observe the impact on fault contributions and OCR performance. Fault resistance values can lead to significant miscoordination or non-tripping events in OCR protection systems. Fault resistance, which occurs when there is an impedance at the fault point, reduces the magnitude of the fault current. As the resistance increases, the fault current decreases, which may cause the OCR to delay tripping or, in some cases, fail to trip altogether. This is because OCRs are designed to operate based on detecting a threshold current value, and if the fault current is reduced due to high resistance, the relay may not identify the situation as a fault, leading to miscoordination. High-resistance faults, particularly those involving arcing, cause a major challenge to traditional OCRs because they produce fault currents that are often too low for detection by conventional settings. In such scenarios, the relay may struggle to differentiate between fault conditions and normal load fluctuations, resulting in either delayed operation or complete failure to trip. This miscoordination can also compromise the reliability of the overall protection scheme, especially in systems with renewable energy sources (PVs), where inverter control methods further complicate fault detection by altering fault current characteristics based on control settings.
- **Data collection:** Collect data on fault contributions, OCR response times, system voltage and current profiles, and overall grid performance.



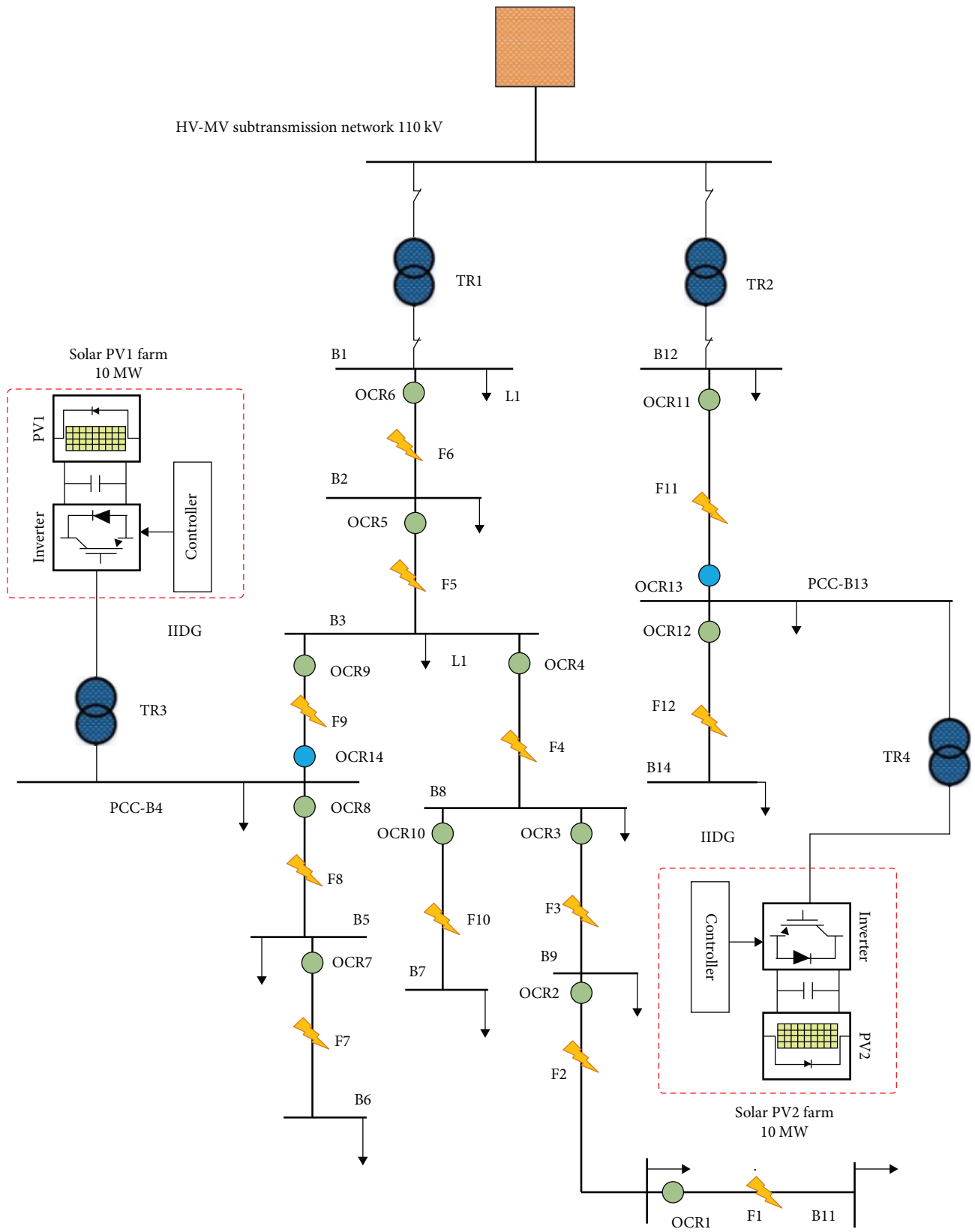


FIGURE 9: The modified 14-bus CIGRE system under study, where the OCR1–12 are nondirectional OCR and OCR13 and OCR14 are directional OCR.



TABLE 3: The fault currents at the CIGRE network's OCRs under different PV control modes, Scenario A.

Fault location	Relays pairs	Control A		Control B		Control C		Control D		Control E	
		$R_f = 0$	$R_f = 5$	$R_f = 0$	$R_f = 5$	$R_f = 0$	$R_f = 5$	$R_f = 0$	$R_f = 5$	$R_f = 0$	$R_f = 5$
F1	OCR1	1820	1317	1820	1317	1734	818	1380	1342	1783	1342
	OCR2	1820	1317	1820	1317	1734	818	1380	1342	1783	1342
F2	OCR2	1956	1172	1956	1172	1827	1061	1476	1354	1814	1743
	OCR3	1956	1172	1956	1172	1827	1061	1476	1354	1814	1743
F3	OCR3	2014	1198	2014	1198	1892	1206	1520	1198	1824	1198
	OCR4	2014	1198	2014	1198	1892	1206	1520	1198	1824	1198
F4	OCR4	2299	1199	2299	1199	2209	1183	1733	589	1784	624
	OCR5	1566	504	1566	504	1568	508	1568	508	1568	508
F5	OCR5	2949	831	2949	831	2949	832	2949	832	2949	826
	OCR6	2949	831	2949	831	2949	832	2949	832	2949	826
F6	OCR6	6711	6697	6711	6697	6711	6711	6711	6711	6711	6711
F7	OCR7	2082	1684	2082	1684	1395	315	1548	1319	1668	1730
	OCR8	2082	1684	2082	1684	1395	315	1548	1319	1668	1730
F8	OCR8	2198	1912	2198	1912	1479	316	1634	1363	1672	1397
	OCR9	1470	1223	1470	1223	1479	316	1470	1222	1470	1222
F9	OCR9	1568	507	1568	507	1568	341	1568	508	1568	508
	OCR5	1568	701	1568	701	1568	341	1568	508	1568	508
F10	OCR14	779	779	779	779	686	650	195	195	253	254
	OCR10	2014	1198	2014	1198	1892	733	1520	1198	1824	1198
F11	OCR4	2014	1198	2014	1198	1892	733	1520	1198	1824	1198
	OCR11	3422	1178	3422	1178	2666	499	2804	558	2837	734
F12	OCR13	2663	501	2663	501	2663	499	2663	500	2663	468
	OCR12	6709	6709	6709	6709	6709	6709	6706	6709	1220	6709
	OCR13	802	364	802	364	48	47	237	379	413	412

- Analysis: Compare the performance of the OCR schemes across different control methods and fault scenarios to evaluate their effectiveness and identify any issues related to fault coordination and grid stability.

4.2.1. Test Results for Scenario A. Table 3 presents the results of the fault currents for different scenarios (locations and fault resistance) and PV control modes, namely Control A, B, C, D, and E. Each fault is protected mainly by primary and backup OCR. The results in Table 3 show a variation in fault currents across various fault locations and PV control modes. For example, in fault F1, OCR1 and OCR2 exhibit lower fault currents under Control D compared to the other controls for  $R_f = 0 \Omega$ , as shown in Figure 10. In Control D, the current-limiting modes of the inverter at  $0.9 < |V_{PCC}^+| \leq 1.1$ , as outlined in the IEEE 1547 standard and described in Equation (5), helped to minimize the high fault values with  $R_f = 0$ . This trend continues at most of the other fault locations except the F11 and F12 at OCR11 and OCR13, where Control C shows a lower fault current. Additionally, Control C shows significantly minimum fault currents compared to other control

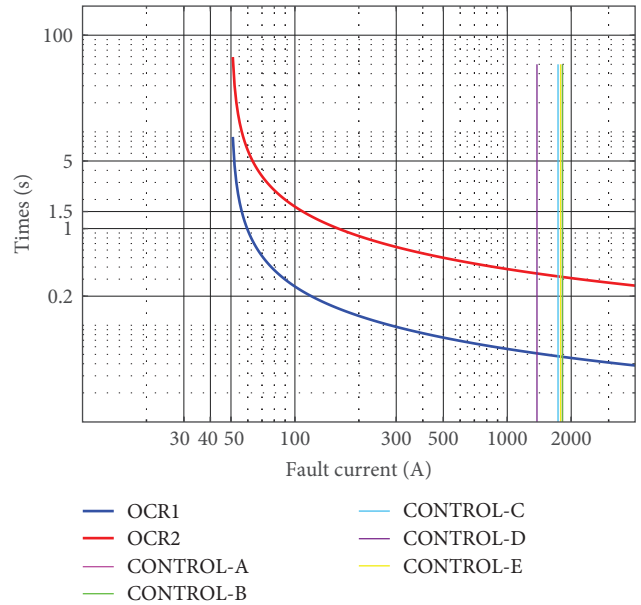


FIGURE 10: The OCR1 and OCR2 schemes under F1 scenario and  $R_f = 0$  for all controllers, Scenario A.

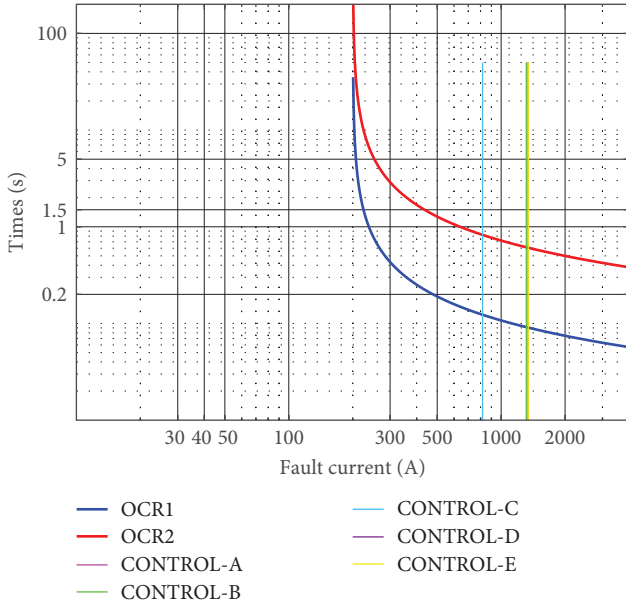


FIGURE 11: The OCR1 and OCR2 schemes under F1 scenario and  $R_f = 5$  for all controllers, Scenario A.

models in the case of the  $R_f = 5 \Omega$ . For example, Control C recorded a minimum fault current (818 A) compared to other controllers at F1, as shown in Figure 11 and Table 3. The control strategy, mode C, is employed to enable the flow of fault current through five different stages, as described in Equation (4). This flexibility in controlling the fault current,  $I_{IIDG}$ , behavior allows for effective adaptation and optimization of the IIDG’s response to various grid conditions, enhancing the overall stability and performance of the system.

The fault currents for Control A and B show similar behavior and results, this is mainly related to the  $V_{PCC}^+$  did not record a value between 0.5 and 0.9, as shown in Table 4, where both controllers worked in the same zone ( $I_{IIDG}$  equal to 2 p.u.), as presented in Figures 2 and 3. Furthermore, Control A and B demonstrates a higher fault current under  $R_f = 0 \Omega$  compared to Control C, D, and E. The PVs contribution to the fault currents is directly related to the  $V_{PCC}^+$  which is varied between the PV system location and control mode, as shown in Table 4. Therefore, Control A and B, as presented in Figures 2 and 3, are fed the grid with maximum fault current from PVs (double the rated current). The PV2 shows significantly higher voltage compared to PV1 in all fault locations except F11 and F12, as these faults are closer to PV1, as shown in Figures 12 and 13. A detailed simulation example, as shown in Figure 14, presents the fault calculation for F1 under Control C and  $R_f = 0$  where the PV1 and PV2 contributes with 638 A ( $V_{PCC}^+ = 0.4$  p.u.) and 256 A ( $V_{PCC}^+ = 1.09$  p.u.), respectively, at the secondary side of the transformer. The total PVs contribution in the fault F1 is 894 A out of the 1734 A. This showed that the control strategies, modes A and B, described by Equations (2) and (3), included a limitation of 2.0 p.u. on the controlled fault current; therefore, they showed similar performance when  $0 \leq |V_{PCC}^+| \leq 0.5$ . In addition, if the bus voltage falls within the range of

1–1.1 p.u., the current is reduced to 1.0 p.u. for both control modes.

This variation in fault currents and voltage levels among OCRs, as shown in Table 4 and Figures 13 and 14, within different fault locations emphasizes the impact of the control model on OCR performance. Table 5 provides the results of the operation time for each OCR under different fault locations and PV control modes. The operation time is measured in seconds and is presented for two fault resistances,  $R_f = 0$  and  $R_f = 5 \Omega$ . Analyzing the results, variations in the operation times across different fault locations and PV control modes are observed. For instance, OCRs at  $R_f = 0$  scenario consistently demonstrates shorter operation times compared to  $R_f = 5$  for all PV control modes. The OCRs operation time for Control A and B shows similar behavior and results, this is mainly related that both modes recorded the same fault level as presented in Table 3. Additionally, Control A and B demonstrate slightly shorter operation times compared to other PV controls. In terms of power protection sensitivity, Control C, D, and E recorded many miscoordination events. For example, Control C at F12 recorded that the backup OCR did not trip and detected the fault at both  $R_f = 0$  and  $R_f = 5 \Omega$  scenarios. This trend continues in Control D and E, where OCR14 did not detect the fault (F9) at both  $R_f = 0$  and  $R_f = 5 \Omega$  scenarios. This is basically due to that the control modes A and B, included a limitation of 2.0 and 1 p.u. on the controlled fault current. The findings emphasize the significance and impact of PV control strategies in achieving optimal operation times for OCRs, thereby improving the overall protection and reliability of power systems. Understanding these variations contributes to the development of efficient and effective control schemes for OCRs, enabling enhanced fault detection and response in power networks.

4.2.2. *Test Results for Scenario B.* Fault currents for different fault scenarios at Scenario B (islanding grid operation mode), including fault locations and fault resistances, under PV control modes A, B, C, D, and E are detailed in Table 6. The results show high variations in fault currents across fault locations over the different control modes at scenario B compared to scenario A, as presented in Table 6. For example, in fault F1, OCR1 and OCR2 exhibit lower fault currents under Control C with 50 A compared to the other controls for  $R_f = 0$  and  $5 \Omega$ , as shown in Figures 15 and 16, respectively. This shows that the fault current, IF, contributed by IIDG is generally within the range of 1.1–2 times the rated current. Moreover, the fault current level depends on factors such as real-time power generation capacity and the location of PV sources. The cumulative effect of these factors can lead to relay misoperation, compromising the security of the system, as well as loss of relay coordination and relay blinding, causing dependability issues.

As the integration of PV systems into DNs increases, understanding the behavior of fault currents under different control modes becomes essential for effective power grid management and protection. Inverter-based resources, such as PV systems, contribute to fault current dynamics in ways that differ significantly from traditional power sources. This

TABLE 4: The voltage ( $V_{PCC}^+$ ) at PV1 and PV2 under different PV control modes, Scenario A.

Fault location	IIDGs	$V_{PCC}^+$ (p.u.)									
		Control A		Control B		Control C		Control D		Control E	
		$R_f = 0$	$R_f = 5$	$R_f = 0$	$R_f = 5$	$R_f = 0$	$R_f = 5$	$R_f = 0$	$R_f = 5$	$R_f = 0$	$R_f = 5$
F1	PV1	0.44	0.44	0.44	0.44	0.4	0.88	0.28	0.36	0.43	0.63
	PV2	1.1	1.1	1.1	1.1	1.09	1.08	1.08	1.08	1.08	1.09
F2	PV1	0.32	0.38	0.32	0.38	0.32	0.79	0.21	0.33	0.32	0.46
	PV2	1.1	1.1	1.1	1.1	1.08	1.08	1.08	1.07	1.08	1.07
F3	PV1	0.15	0.32	0.15	0.32	0.29	0.73	0.18	0.71	0.27	0.71
	PV2	1.09	1.09	1.09	1.09	1.07	1.07	1.07	1.08	1.07	1.09
F4	PV1	0.15	0.15	0.15	0.15	0.13	0.13	0.04	0.03	0.05	0.05
	PV2	1.08	1.08	1.08	1.08	1.1	1.1	1.1	1.1	1.07	1.09
F5	PV1	0.4	0.4	0.4	0.4	0.31	0.77	0.1	0.1	0.26	0.77
	PV2	1	1	1	1	1.04	1.04	1.04	1.07	1.1	1.07
F6	PV1	0.49	0.49	0.49	0.49	0.41	0.07	0.14	0.3	0.49	0.93
	PV2	1	1	1	1	0.96	0.96	0.96	0.96	1.04	0.46
F7	PV1	0.16	0.19	0.16	0.19	0.05	0.006	0.09	0.34	0.12	0.45
	PV2	1.05	1.05	1.05	1.05	1.07	1.07	1.07	1.07	1.07	1.07
F8	PV1	0.12	0.12	0.12	0.12	0.005	0.2	0.03	0.03	0.03	0.03
	PV2	1.09	1.09	1.09	1.09	1.07	1.07	1.07	1.07	1.07	1.07
F9	PV1	0.15	0.15	0.15	0.15	0.13	0.59	0.03	0.03	0.05	0.05
	PV2	1.09	1.09	1.09	1.09	1.1	1.1	1.1	1.09	1.1	1.1
F10	PV1	0.28	0.32	0.28	0.32	0.29	1.1	0.18	0.71	0.27	0.71
	PV2	1.1	1.1	1.1	1.1	1.07	1.1	1.1	1.08	1.07	1.09
F11	PV1	1.1	1.06	1.1	1.06	1.04	1.04	1.04	1.1	1.04	1.1
	PV2	0.12	0.12	0.12	0.12	0.06	0.006	0.03	0.03	0.03	0.95
F12	PV1	1.1	1.07	1.1	1.07	0.98	1.1	0.98	1.1	0.98	1.05
	PV2	0.3	0.3	0.3	0.3	0.01	0.09	0.08	0.3	0.05	0.15

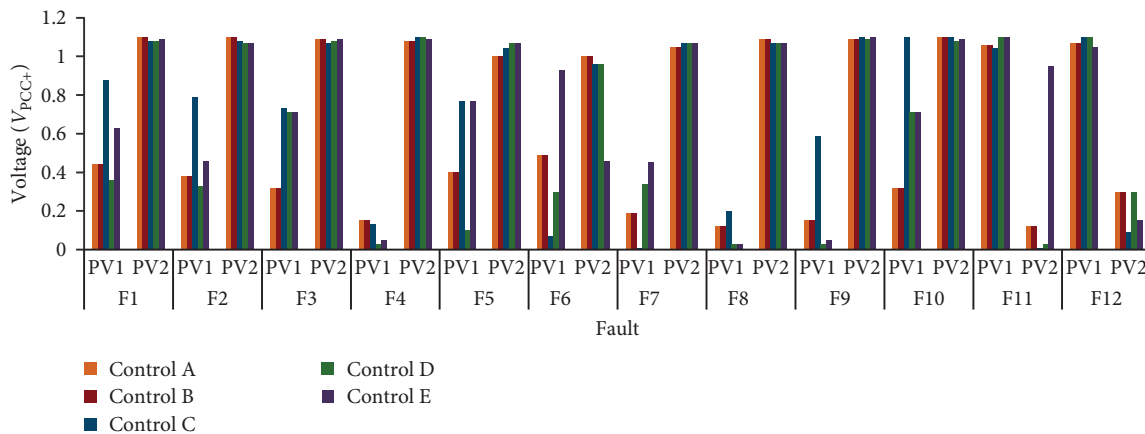


FIGURE 12: The voltage ( $V_{PCC}^+$ ) at PV1 and PV2 under different PV control modes, Scenario A with  $R_f = 0$ .

creates challenges for OCR coordination and grid stability, especially when various control strategies are employed:

- First, the fault currents for Control A and B at scenario B did not show similar behavior and results as scenario A, which can be attributed to the fact that the  $V_{PCC}^+$  record values between 0.5 and 0.9, as shown in Table 7.

- Second, Control D and E show significantly lower fault currents compared to Control A and B at  $R_f = 0$  and  $R_f = \Omega$ , as presented in Table 6. Control C demonstrates minimum fault currents at  $R_f = 0 \Omega$  and  $R_f = 5$  compared to Control A, B, D, and E. These variations are influenced by the contribution of PV systems, indicated by  $V_{PCC}^+$ , as detailed in Table 7, which differs

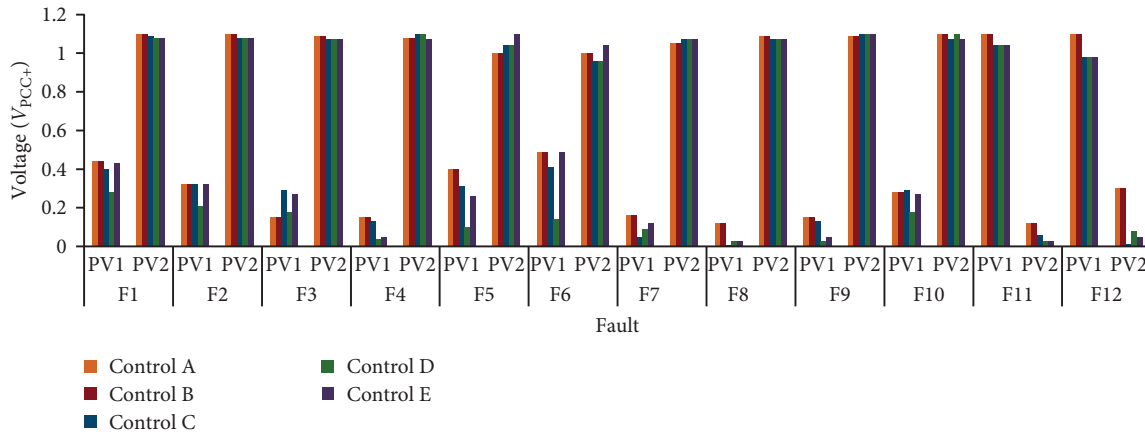


FIGURE 13: The voltage ( $V_{PCC}^+$ ) at PV1 and PV2 under different PV control modes, Scenario A with  $R_f = 5$ .

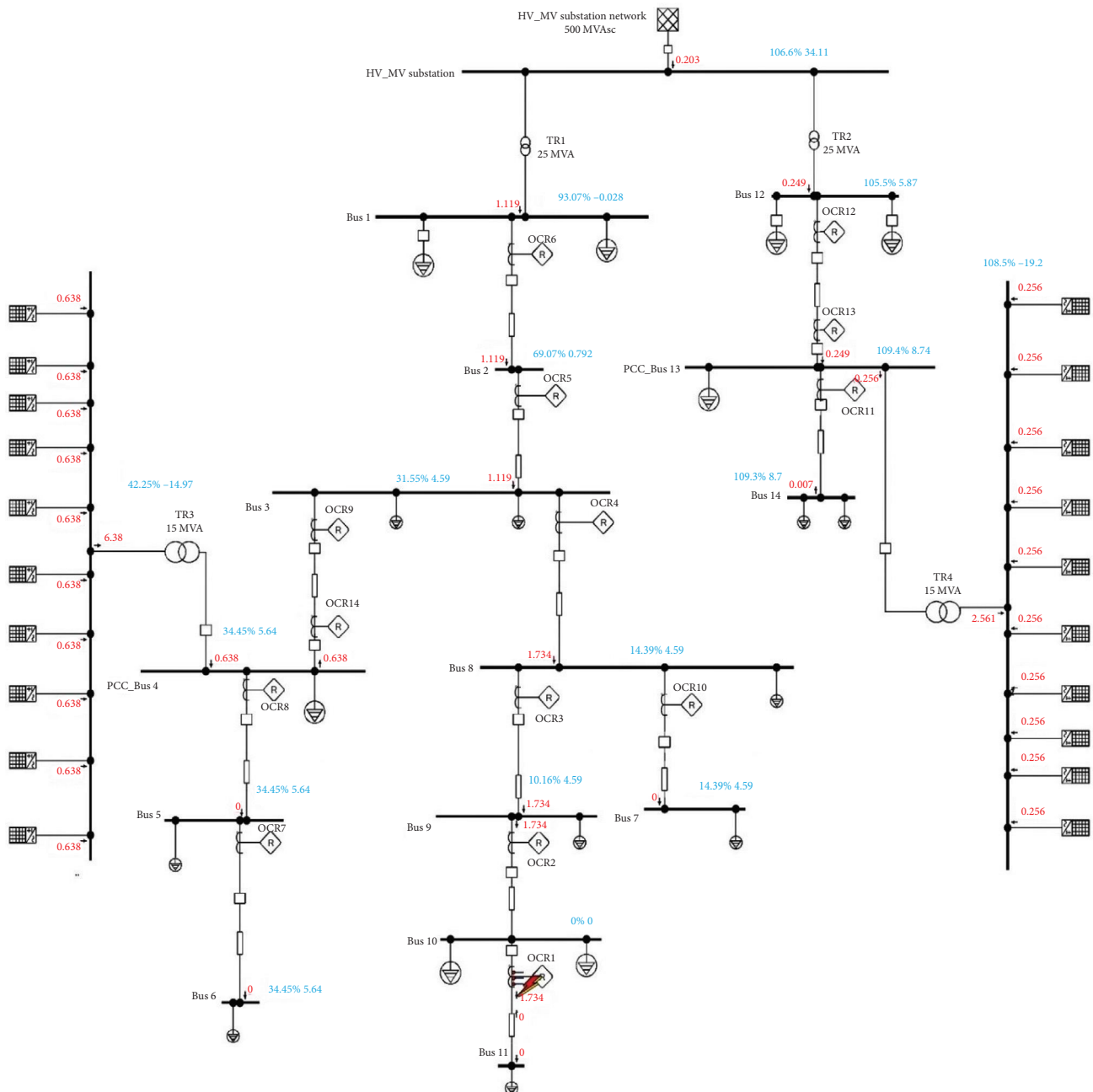


FIGURE 14: The fault current results for the F1 scenario under Control C and  $R_f = 0$ , Scenario A.

TABLE 5: The operational time for OCR (second) at the CIGRE network under different PV control modes, Scenario A.

Fault location	Relays pairs	Operational time for OCR (s)									
		Control A		Control B		Control C		Control D		Control E	
		$R_f = 0$	$R_f = 5$	$R_f = 0$	$R_f = 5$	$R_f = 0$	$R_f = 5$	$R_f = 0$	$R_f = 5$	$R_f = 0$	$R_f = 5$
F1	OCR1	0.05	0.05	0.05	0.05	0.05	0.06	0.05	0.05	0.05	0.05
	OCR2	0.33	0.37	0.33	0.37	0.34	0.43	0.36	0.36	0.36	0.36
F2	OCR2	0.33	0.38	0.33	0.38	0.33	0.39	0.35	0.36	0.35	0.36
	OCR3	0.59	0.69	0.59	0.69	0.60	0.71	0.64	0.66	0.64	0.66
F3	OCR3	0.59	0.69	0.59	0.69	0.60	0.68	0.64	0.69	0.64	0.69
	OCR4	0.85	1.00	0.85	1.00	0.87	1.00	0.93	1.00	0.93	1.00
F4	OCR4	1.01	1.00	1.01	1.00	1.03	1.00	1.12	1.81	1.12	1.81
	OCR5	1.45	2.85	1.45	2.85	1.45	2.83	1.45	2.83	1.45	2.83
F5	OCR5	1.14	2.00	1.14	2.00	1.14	2.00	1.14	2.00	1.14	2.00
	OCR6	1.43	2.53	1.43	2.53	1.43	2.53	1.43	2.53	1.43	2.53
F6	OCR6	1.12	1.12	1.12	1.12	1.12	1.12	1.12	1.12	1.12	1.12
F7	OCR7	0.05	0.05	0.05	0.05	0.05	0.09	0.05	0.05	0.05	0.05
	OCR8	0.31	0.33	0.31	0.33	0.35	0.64	0.34	0.35	0.34	0.35
F8	OCR8	0.31	0.32	0.31	0.32	0.34	0.64	0.33	0.35	0.33	0.35
	OCR9	0.64	0.68	0.64	0.68	0.64	1.19	0.64	0.68	0.64	0.68
F9	OCR9	0.63	0.94	0.63	0.94	0.63	1.14	0.63	0.94	0.63	0.94
	OCR5	0.98	1.29	0.98	1.29	0.98	1.78	0.98	1.47	0.98	1.47
F10	OCR14	0.18	0.18	0.18	0.18	0.21	0.22	No tripping	No tripping	No tripping	No tripping
	OCR10	0.05	0.05	0.05	0.05	0.05	0.06	0.05	0.05	0.05	0.05
F11	OCR4	0.85	1.00	0.85	1.00	0.87	1.19	0.93	1.00	0.88	1.00
	OCR11	0.05	0.07	0.05	0.07	0.05	0.11	0.05	0.10	0.05	0.09
F12	OCR12	0.35	0.72	0.35	0.72	0.35	0.72	0.35	0.72	0.35	0.75
	OCR12	0.33	0.33	0.33	0.33	0.33	0.33	0.33	0.33	0.56	0.33
F12	OCR13	0.18	0.9	0.18	0.9	No tripping	No tripping	No tripping	0.75	0.55	0.55

based on the PV system location and control mode. Except F11 and F12, which are closer to PV1 than PV2, as seen in Figures 17 and 18, PV2 shows a significantly higher voltage than PV1 in all fault sites. A detailed simulation example, as shown in Figure 19, presents the fault calculation for F1 under Control C and  $R_f = 5$  where the PV1 and PV2 contributes with 4 A ( $V_{PCC}^+ = 0.02$  p.u.) and 46 A ( $V_{PCC}^+ = 0.06$  p.u.), respectively, at the secondary side of the transformer. The total PVs contribution in feeding the system and the fault F1 is 50 A. The PVs contribution to the fault currents by Control C is directly related to the  $V_{PCC}^+$  which is at the most fault locations are lower than 0.1 p.u. This leads to having a minimum  $I_{IIDG}$  and close to zero based on the Control C model, as described by Equation (4) and Figure 4.

The variation in fault currents and voltage levels among OCRs, as depicted in Tables 6 and 7, highlights the influence of control models on OCR performance. Table 8 presents operation time results for each OCR under different fault locations and PV control modes, measured in seconds for  $R_f = 0$  and  $R_f = 5 \Omega$  scenarios. OCRs at Control A and B outperform the other controllers in terms of high protection sensitivity with minimum miscoordination events, as shown in Table 8. The fault current values for Control C at  $R_f = 0$

and  $R_f = 5 \Omega$  was significantly low, which resulted in difficulties in fault detecting and led to instances of no tripping and miscoordination events. The control mode C, is developed to enable the flow of fault current through five different stages, as described in Equation (4). This flexibility in controlling the fault current,  $I_{IIDG}$ , behavior allows for effective adaptation and optimization of the IIDG's response to various grid conditions, enhancing the overall stability and performance of the system. This trend continues with Control D and E where OCR14 fails to detect the fault (F9) at  $R_f = 0$ . These findings underscore the significance of PV control strategies in achieving optimal OCR operation times and enhancing the protection and reliability of power systems. In addition, OCRs at  $R_f = 0$  consistently exhibits shorter operation times compared to  $R_f = 5$  across all PV control modes.

### 4.3. Discussion

**4.3.1. Mismatch Events.** The results obtained from the analysis showed instances of OCR miscoordination and no tripping events, highlighting the significance of proper coordination among OCRs in power systems with PVs. Particularly, Control C, D, and E demonstrated a challenge in fault detecting at  $R_f = 0$  and  $5 \Omega$  for both grid operation Scenarios A and B, where the no tripping events have occurred many times. This is mainly attributed to the low fault current



TABLE 6: The fault currents at the CIGRE network's OCRs under different PV control modes, Scenario B.

Fault location	Relays pairs	Control A		Control B		Control C		Control D		Control E	
		$R_f = 0$	$R_f = 5$	$R_f = 0$	$R_f = 5$	$R_f = 0$	$R_f = 5$	$R_f = 0$	$R_f = 5$	$R_f = 0$	$R_f = 5$
F1	OCR1	1505	1012	1307	1317	50	50	422	402	955	943
	OCR2	1505	1,012	1307	1317	50	50	422	402	955	943
F2	OCR2	1221	1203	1354	1699	50	50	423	424	858	1125
	OCR3	1221	1203	1354	1699	50	50	423	424	858	1125
F3	OCR3	1590	924	1524	1179	50	50	423	394	772	868
	OCR4	1590	924	1524	1179	50	50	423	394	772	868
F4	OCR4	1350	1119	1541	1199	717	1049	429	452	714	761
	OCR5	726	1119	651	504	46	342	230	342	533	260
F5	OCR5	773	443	773	831	47	50	233	231	637	443
	OCR6	773	443	773	831	50	50	233	231	509	443
F6	OCR6	726	650	726	6697	47	50	234	234	725	727
	OCR7	1220	1205	1433	1684	50	50	424	484	708	961
F7	OCR8	1220	1205	1433	1684	50	50	424	484	708	961
	OCR8	1280	998	1415	1912	50	50	424	422	690	660
F8	OCR9	1508	298	1415	1223	46	50	229	422	521	494
	OCR9	726	1272	624	507	46	342	230	275	533	342
F9	OCR5	726	1272	624	701	46	342	230	275	533	342
	OCR14	779	490	701	779	686	713	195	195	253	312
F10	OCR10	1590	924	1524	1179	50	50	423	424	772	868
	OCR4	1590	924	1524	1179	50	50	423	424	772	868
F11	OCR11	1500	538	1390	1178	517	571	390	553	679	612
	OCR12	500	226	685	501	515	249	195	223	515	266
F12	OCR12	683	520	672	6709	571	359	195	276	578	547
	OCR13	779	364	390	364	48	46	237	236	416	413

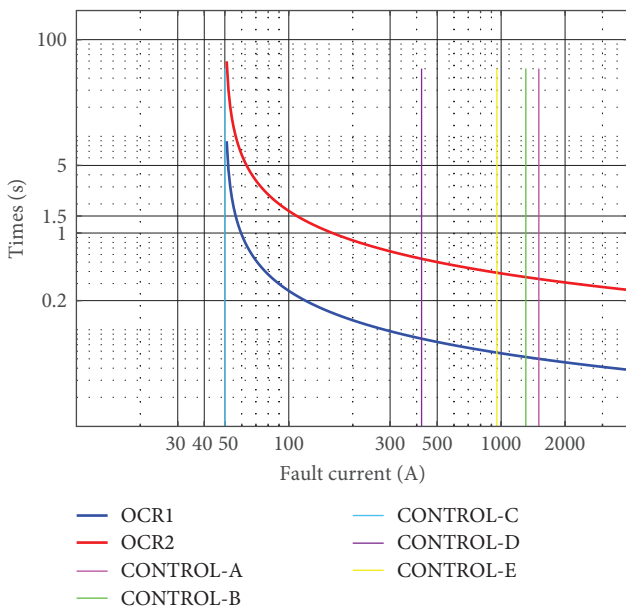


FIGURE 15: The OCR1 and OCR2 schemes under F1 scenario and  $R_f = 0$  for all controllers, Scenario B.

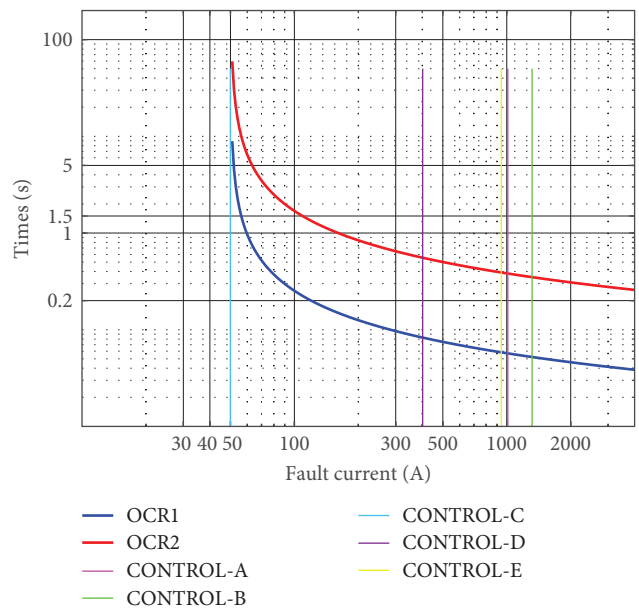


FIGURE 16: The OCR1 and OCR2 schemes under F1 scenario and  $R_f = 5$  for all controllers, Scenario B.

TABLE 7: The voltage ( $V_{PCC}^+$ ) at PV1 and PV2 under different PV control modes, Scenario B.

Fault location	Relays pairs	Control A		Control B		Control C		Control D		Control E	
		$R_f = 0$	$R_f = 5$	$R_f = 0$	$R_f = 5$	$R_f = 0$	$R_f = 5$	$R_f = 0$	$R_f = 5$	$R_f = 0$	$R_f = 5$
F1	PV1	0.36	0.43	0.36	0.44	0.009	0.02	0.11	0.21	0.27	0.59
	PV2	0.66	1.1	0.66	1.1	0.057	0.06	0.33	0.91	0.7	0.78
F2	PV1	0.29	0.3	0.29	0.39	0.006	0.01	0.08	0.13	0.18	0.47
	PV2	0.62	1.09	0.62	1.1	0.05	0.05	0.31	0.88	0.66	0.72
F3	PV1	0.26	0.48	0.26	0.33	0.056	0.02	0.07	0.25	0.14	0.64
	PV2	0.61	1.09	0.61	1.09	0.053	0.06	0.3	0.92	0.65	0.8
F4	PV1	0.15	0.13	0.15	0.15	0.13	0.14	0.038	0.03	0.05	0.6
	PV2	0.54	1.1	0.54	1.08	0.04	0.85	0.26	0.85	0.62	1.01
F5	PV1	0.4	0.36	0.4	0.4	0.31	0.77	0.1	0.39	0.26	0.81
	PV2	0.44	0.84	0.44	1	0.03	0.07	0.19	0.37	0.53	0.72
F6	PV1	0.49	0.49	0.49	0.49	0.41	0.8	0.14	0.93	0.49	0.96
	PV2	0.35	0.92	0.35	1	0.02	0.02	0.14	0.14	0.45	0.45
F7	PV1	0.17	0.28	0.17	0.19	0.002	0.01	0.04	0.14	0.07	0.26
	PV2	0.59	0.78	0.59	1.05	0.052	0.05	0.14	0.81	0.64	0.73
F8	PV1	0.12	0.3	0.12	0.12	0.0006	0.0006	0.03	0.03	0.03	0.03
	PV2	0.63	0.93	0.63	1.09	0.02	0.05	0.27	0.48	0.63	0.66
F9	PV1	0.15	0.1	0.15	0.15	0.13	0.23	0.03	0.07	0.05	0.1
	PV2	0.62	0.9	0.62	1.09	0.048	0.85	0.26	0.96	0.62	0.85
F10	PV1	0.27	0.65	0.27	0.32	0.005	0.02	0.07	0.13	0.14	0.64
	PV2	0.67	1.04	0.67	1.1	0.053	0.06	0.3	0.88	0.65	0.8
F11	PV1	0.62	0.72	0.62	1.06	0.62	1.1	0.23	1.1	0.62	1
	PV2	0.12	1.1	0.12	0.12	0.006	0.77	0.03	0.75	0.03	0.81
F12	PV1	0.57	0.56	0.57	1.07	0.55	0.81	0.19	0.97	0.15	0.59
	PV2	0.3	0.78	0.3	0.3	0.013	0.09	0.08	0.08	0.56	0.15

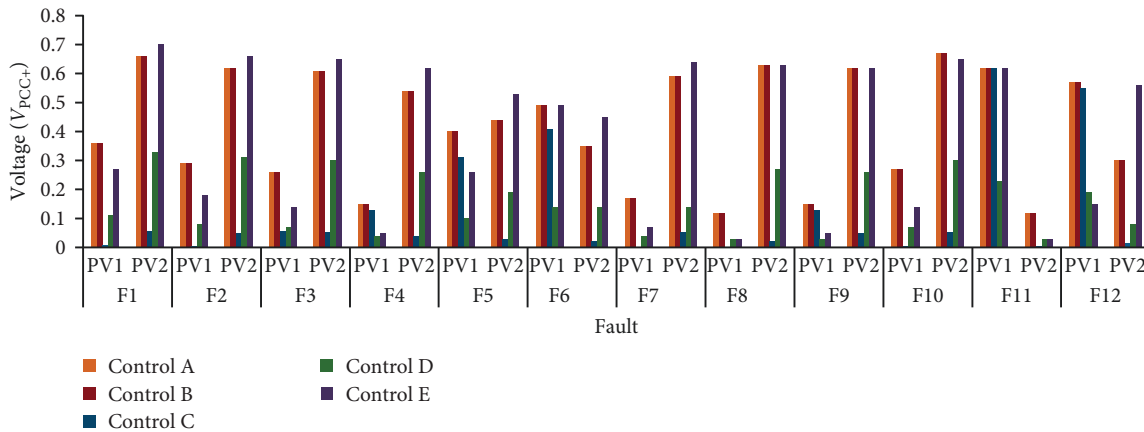


FIGURE 17: The voltage ( $V_{PCC}^+$ ) at PV1 and PV2 under different PV control modes, Scenario B with  $R_f = 0$ .

values observed when employing these controllers, which limit the contribution of PV currents and lead to difficulties in accurately detecting and isolating faults, resulting in no trip events. For example, Figure 20 illustrates the misoperation of OCRs event for OCR1 and OCR2 in Scenario B when a fault occurs at location F1, under Control C and  $R_f = 0$ . In this scenario, the primary relay OCR1 and backup relay OCR2 failed to operate as the fault current (49.8 A) was

lower than the OCR scheme setting. These events heighten the danger of equipment damage and system instability.

Additionally, Control C, D, and E posed challenges in maintaining the CTI at Scenario A within an acceptable range of 0.2–0.5 s, leading to miscoordination events. In Scenario B, all PV inverter controllers caused the same miscoordination events with a CTI of more than 0.5. For instance, in Scenario A with a fault occurring at location F4 under Control D and

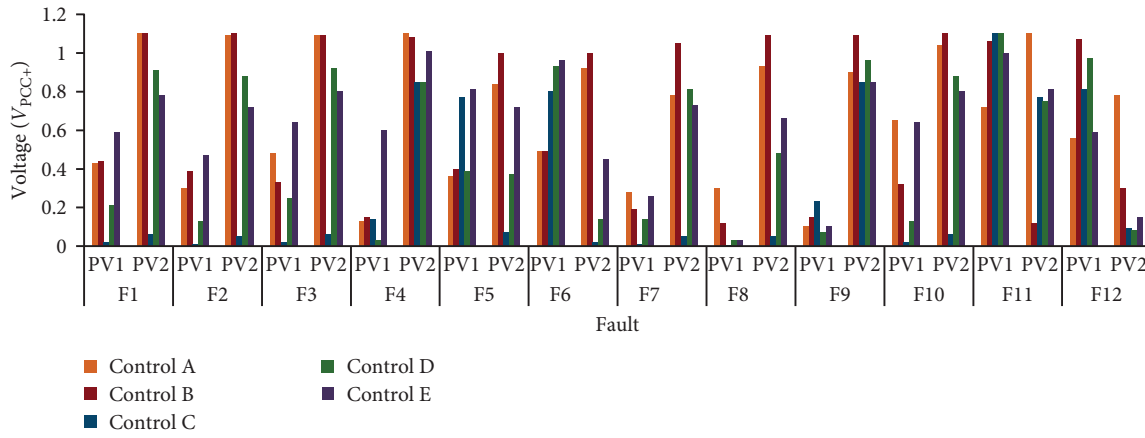


FIGURE 18: The voltage ( $V_{PCC}^+$ ) at PV1 and PV2 under different PV control modes, Scenario B with  $R_f = 5$ .

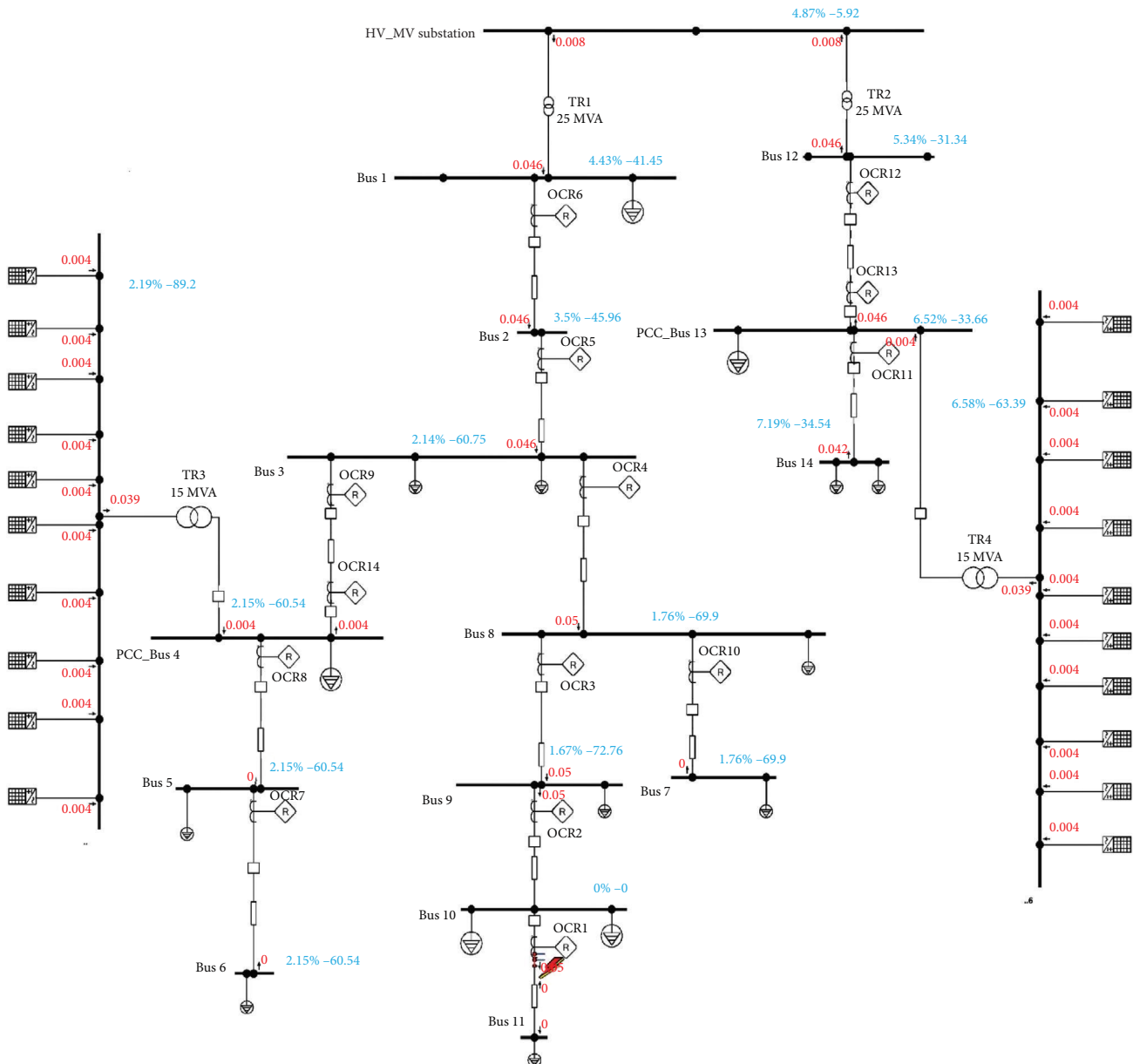


FIGURE 19: The fault current results for the F1 scenario under Control C and  $R_f = 5$ , Scenario B.

TABLE 8: The operational time for OCR (second) at the CIGRE network under different PV control modes, Scenario B.

Fault location	Relays pairs	Control A		Control B		Control C		Control D		Control E	
		$R_f = 0$	$R_f = 5$	$R_f = 0$	$R_f = 5$	$R_f = 0$	$R_f = 5$	$R_f = 0$	$R_f = 5$	$R_f = 0$	$R_f = 5$
F1	OCR1	0.05	0.06	0.05	0.05	No tripping	No tripping	0.08	0.08	0.06	0.06
	OCR2	0.35	0.40	0.37	0.37	No tripping	No tripping	0.57	0.58	0.41	0.41
F2	OCR2	0.35	0.38	0.36	0.34	No tripping	No tripping	0.57	0.57	0.42	0.39
	OCR3	0.63	0.69	0.66	0.62	No tripping	No tripping	1.03	1.03	0.77	0.70
F3	OCR3	0.63	0.75	0.64	0.69	No tripping	No tripping	1.03	1.07	0.80	0.77
	OCR4	0.91	1.09	0.93	1.00	No tripping	No tripping	1.50	1.55	1.16	1.11
F4	OCR4	1.14	1.32	1.16	1.00	1.63	1.36	2.21	2.14	1.63	1.58
	OCR5	2.18	1.70	2.34	2.85	No tripping	4.2	8.13	4.20	2.72	6.31
F5	OCR5	2.09	3.19	2.09	2.00	No tripping	No tripping	7.89	8.05	2.38	3.19
	OCR6	2.64	4.02	2.64	2.53	No tripping	No tripping	9.95	10.15	3.56	4.02
F6	OCR6	2.75	2.96	2.75	1.12	No tripping	No tripping	9.86	9.86	2.75	2.75
	OCR7	0.05	0.05	0.05	0.05	No tripping	No tripping	0.08	0.08	0.06	0.06
F7	OCR8	0.34	0.36	0.35	0.33	No tripping	No tripping	0.55	0.52	0.44	0.39
	OCR8	0.34	0.39	0.35	0.32	No tripping	No tripping	0.55	0.55	0.44	0.45
F8	OCR9	0.64	1.23	0.65	0.68	No tripping	No tripping	1.45	1.03	0.93	0.96
	OCR9	0.82	0.67	0.87	0.94	No tripping	1.14	1.45	1.29	0.92	1.14
F9	OCR5	1.27	1.04	1.35	1.29	No tripping	1.78	2.25	2.01	1.44	1.78
	OCR14	0.18	0.35	0.20	0.18	0.21	0.2	No tripping	No tripping	No tripping	4.46
F10	OCR10	0.05	0.06	0.05	0.05	No tripping	No tripping	0.08	0.08	0.06	0.06
	OCR4	0.91	1.09	0.93	1.00	No tripping	No tripping	1.50	1.50	1.16	1.11
F11	OCR11	0.06	0.10	0.06	0.07	No tripping	0.1	0.13	0.10	0.09	0.09
	OCR12	0.58	1.43	0.60	0.72	No tripping	1.28	1.75	1.45	0.71	1.19
F12	OCR12	0.71	0.86	0.74	0.33	0.81	1.1	2.14	1.40	0.80	0.83
	OCR13	0.18	0.9	0.67	0.9	No tripping	No tripping	No tripping	No tripping	0.53	0.55

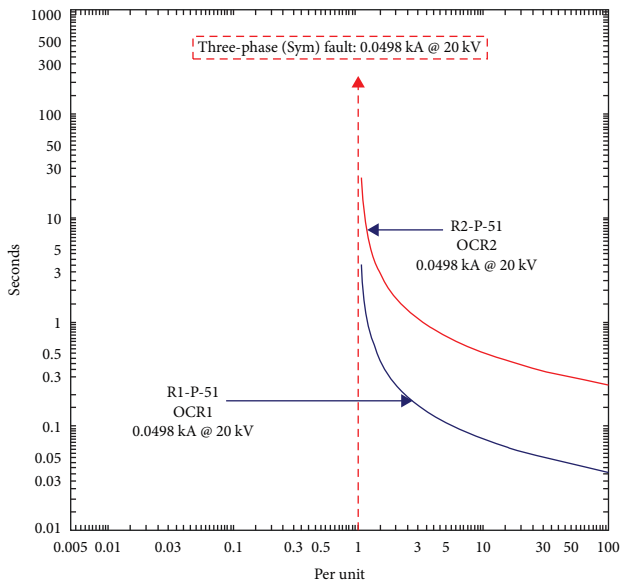


FIGURE 20: Characteristics curves of OCR1 and OCR2 fault current results for F1 scenario under Control C and  $R_f = 0$ , Scenario B.

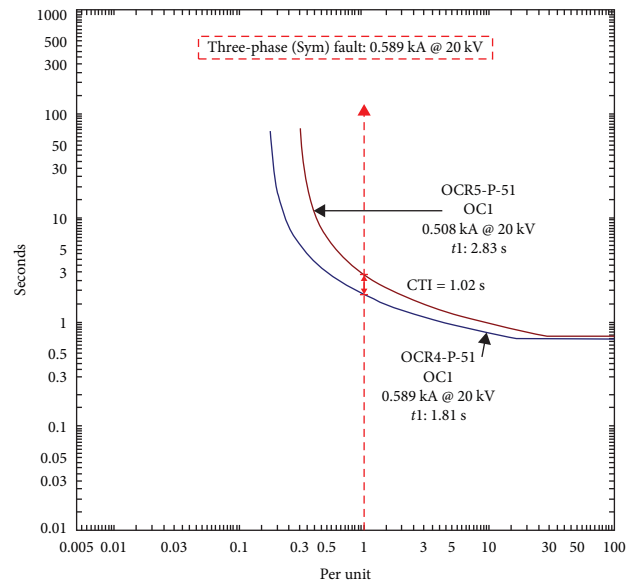


FIGURE 21: Characteristics curves of OCR4 and OCR5 fault current results for F4 scenario under Control D and  $R_f = 5$ , Scenario A.

$R_f = 5 \Omega$ , the misoperation of OCRs, specifically OCR4 and OCR5, is evident as depicted in Figure 21. In this situation, the backup relay OCR5 failed to activate within the standard CTI and was delayed by 1.02 s. The CTI is a critical parameter that

determines the time delay between the operation of primary and backup OCRs. In this case, the CTI exceeded the recommended range, indicating a deviation from the desired coordination scheme. These miscoordination events can result

in delayed fault clearing, false tripping, and overall compromise of the system’s reliability and security. It is essential to address these challenges and optimize the control strategies to ensure effective coordination and timely fault response of OCRs in power systems with PVs.

In general, as renewable energy integration into the grid continues to expand, managing both active and reactive power during fault conditions has become increasingly important. Various control methods, as outlined in Table 1, have been developed to improve grid flexibility. This study examined the most widely used control methods, Control A, B, C, D, and E, including those implemented in the Germany grid code and IEEE 1547:2018, as well as other commonly employed techniques. The results showed that the inverter control schemes have a substantial impact on the performance of OCR schemes in both grid connected and islanding operation modes. The contribution of fault current from inverter-based systems is heavily influenced by the control strategy employed. In grid-connected mode, the fault current is a combination of contributions from both the utility grid and inverter-based resources. Different control schemes influence the magnitude of this contribution. OCR schemes, which rely on fault current detection, may struggle to adapt to this variability. This results in unreliable operation, leading to unnecessary or missed disconnections, thereby affecting system reliability. In islanding mode, where only PV systems are powering the network, the role of the inverter control becomes even more critical. Since the grid is disconnected, the entire fault current contribution relies on the inverters. If the control scheme of the inverter limits or eliminates the fault current, the OCR may completely fail to detect the fault due to insufficient current to trigger a response. This creates a higher risk in islanding scenarios, where protection systems are already more vulnerable due to the absence of grid support. In such cases, the OCR may not trip at all, leaving the system in an unsafe state. Inverter control schemes play a crucial role in determining fault current contributions, with control strategies that reduce or eliminate fault currents significantly impacting OCR performance. The variability introduced by different inverter control schemes presents challenges for traditional OCR systems, especially in islanding mode, where fault detection relies entirely on inverter-generated current. Adaptive OCR schemes are needed to address these challenges and ensure effective protection across varying control modes.

**4.3.2. Modern OCR Schemes.** Several optimization techniques have been explored in the literature to address the challenge of coordinating overcurrent protection schemes, as discussed in Sections 1 and 3. The WCA and PSO have demonstrated effectiveness in solving complex power network and protection problems. The choice of these two optimization algorithms is based on their reputation as powerful and effective methods for tackling complex power protection problems. PSO is a popular and well-established method due to its simplicity and effectiveness. However, PSO has its limitations, particularly its tendency to become trapped in local minima, which can limit its ability to find global optimal solutions in complex optimization problems. Despite these

limitations, PSO remains widely used because of its robustness and efficiency in many engineering applications, including OCR coordination. It provides a good balance between computational complexity and solution quality, making it a reliable benchmark for comparison. On the other hand, the WCA is a relatively newer approach that mimics the natural water cycle process. WCA has gained attention due to its ability to explore and exploit the search space more effectively than standard PSO. The main advantage of WCA is its dynamic adaptation mechanism, which allows it to avoid local minima by directing its search toward the global optimum. This makes WCA particularly suitable for complex optimization problems with large search spaces, such as OCR coordination with renewable energy integration. In this study, WCA was chosen alongside PSO to compare their performance in handling various inverter control schemes and grid operation scenarios. While PSO serves as a reliable reference point, WCA was selected for its enhanced global search capability and adaptability, addressing some of PSO’s well-known limitations. By comparing both PSO and WCA, the study aims to provide insights into their effectiveness in achieving optimal OCR coordination under different fault conditions and inverter control modes, helping to identify the most suitable approach for modern power grids with distributed generation.

By employing these algorithms, the potential impact of PV inverter Control A on fault contribution and relay settings is evaluated. Control A showed higher performance in terms of minimum miscoordination events. Specifically, the focus is on minimizing the total tripping time, a critical metric for assessing the performance of coordination schemes. The results presented in Table 9 display the total operating time for OCRs under Scenario A with Control A and  $R_f = 0$ , considering both nonstandard and standard tripping characteristics. The optimization algorithms, PSO and WCA, are employed to determine the TMS values for each OCR. When examining the TMS values, it is observed that for OCRs 1, 7, 10, and 11, consistent TMS values of 0.025 are achieved across both the nonstandard and standard tripping schemes by both PSO and WCA. This indicates the effective coordination and minimal time margin required for these relays. For other OCRs, the TMS values vary between the nonstandard and standard tripping schemes. The optimization algorithms successfully determine TMS values that provide efficient coordination and minimize the operating time for these relays under both schemes. Analyzing the total operating time, the total operating time for the nonstandard tripping scheme was 12.077–12.3003 s for PSO and WCA, respectively, while for the standard tripping scheme, it was 12.1226 and 12.1564 s. By selecting the most appropriate coordination approach, network operators can enhance the overall performance and reliability of the power system, ensuring effective fault detection and response.

**4.4. HIL Testing Results.** HIL testing is a powerful method for evaluating hardware components in simulated conditions, especially in power systems and control engineering. This research uses HIL testing to tackle the issue of fault currents in microgrids with different PV control modes. It proposes a



TABLE 9: The TMS and total operational time for OCR (second) at the CIGRE network under Control A, Scenario A for WCA and PSO optimization algorithms, and nonstandard and standard tripping characteristics.

Relay	TMS of OCRs at Scenario A under Control A and $R_f = 0$			
	Nonstandard		Standard	
	PSO	WCA	PSO	WCA
OCR1	0.025	0.025	0.025	0.025
OCR2	0.2837	0.228252	0.1771	0.177594
OCR3	0.4999	0.444859	0.321561	0.322452
OCR4	0.7221	0.667741	0.467565	0.468651
OCR5	0.686	0.643163	0.498621	0.499809
OCR6	0.8523	0.809807	0.629037	0.630587
OCR7	0.025	0.025115	0.025	0.025
OCR8	0.2499	0.250679	0.171311	0.171699
OCR9	0.488	0.489533	0.32016	0.320953
OCR10	0.0251	0.025	0.025045	0.025
OCR11	0.0251	0.025	0.025	0.025821
OCR12	0.2369	0.240647	0.168004	0.169203
Total operating time	12.077	12.3003	12.1226	12.1564

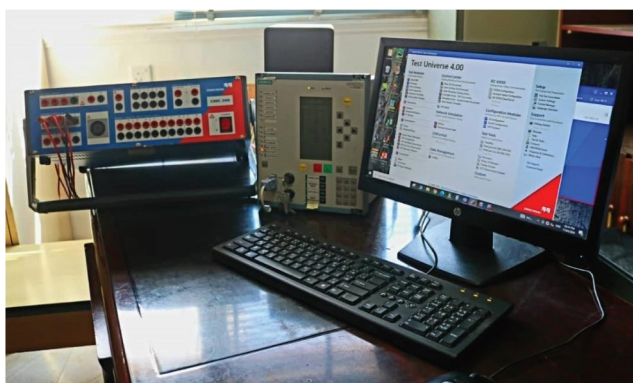


FIGURE 22: Hardware components of HIL.

TABLE 10: The fault currents simulated and injected to OCR under different PV control modes, Scenario B.

Fault location	Relays pairs	Fault current (A)				
		Control A	Control B	Control C	Control D	Control E
F1	OCR2	1012	1317	50	402	943

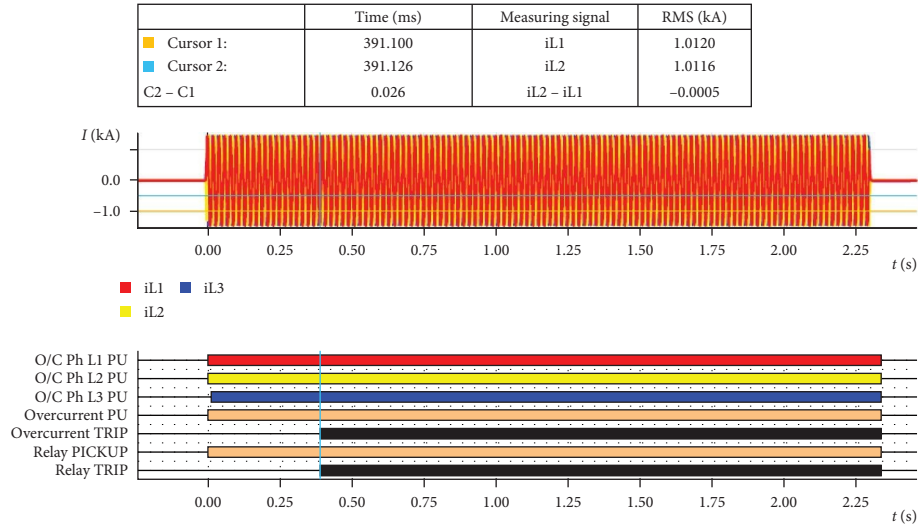
unique protection scheme with nonstandard characteristics for industrial relays, offering adaptability for different manufacturers. IL testing involves integrating physical hardware components like SIPROTEC 7SJ62 multifunction protection relay and OMICRON-CMC-365 with simulation software, as shown in Figure 22. The key steps are as follows:

- Simulation software: Models power system components using ETAP and ATP/EMTP simulations and performs load flow and short-circuit calculations.
- Hardware components: Connects SIPROTEC 7SJ62 and OMICRON-CMC-365 to the HIL setup, with

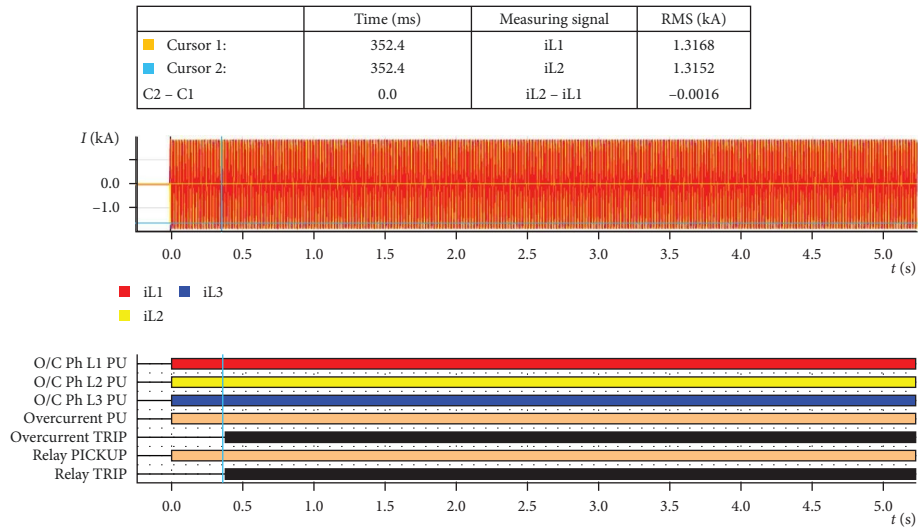
ATP simulations sending test data to these devices for real-world validation.

- Real-time simulation platform: Uses OMICRON Test Universe software for control and synchronization, and Digsig Software for OCR programming and validation.

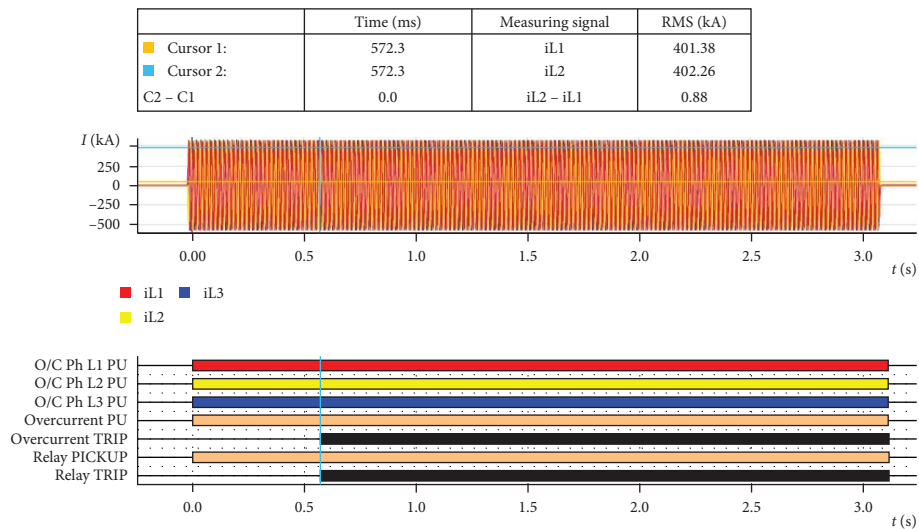
This setup allows to assess the effectiveness of the protection scheme, providing a robust platform to ensure safety and reliability in microgrid environments. In the HIL testing, fault currents for different fault scenarios at Scenario B (islanding grid operation mode), including fault location



(a)



(b)



(c)

FIGURE 23: Continued.

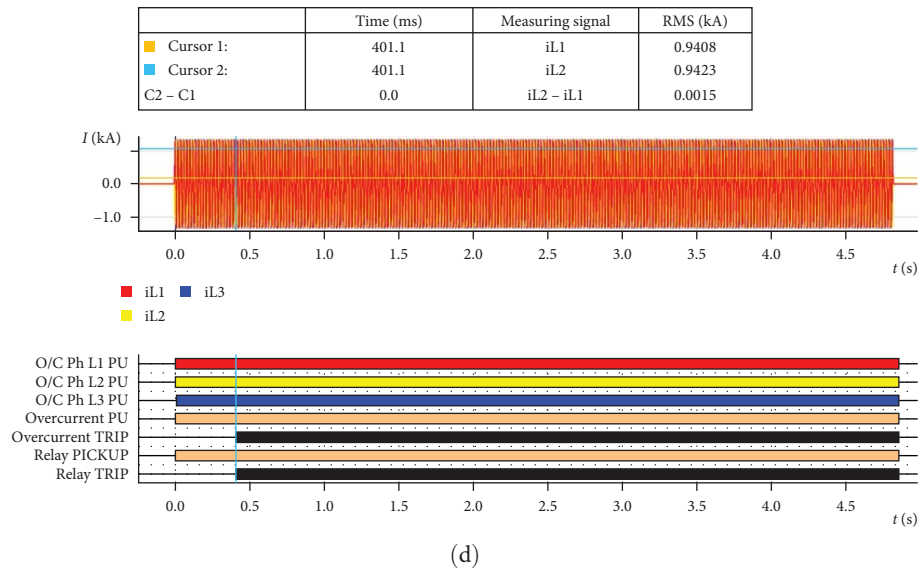


FIGURE 23: HIL testing results for OCR2 under F1 as detailed in Table 10 for (a) Control A, (b) Control B, (c) Control D, and (d) Control E.

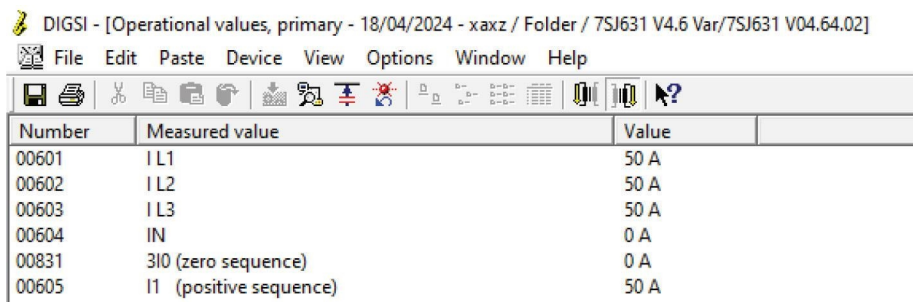


FIGURE 24: HIL testing results for OCR2 under F1 as detailed in Table 10 for Control C, where the relay did not operate.

(F1) and fault resistances ( $5 \Omega$ ), under PV control modes A, B, C, D, and E are detailed in Table 10.

In this study, we utilized HIL testing to evaluate the performance of a protection scheme in a microgrid environment. Table 10 details fault currents observed in Scenario B, which represents an islanded grid operation mode. The data include fault location (F1) with a fault resistance of  $5 \Omega$ , under different PV control modes: A, B, C, D, and E for OCR2. The results from HIL testing discovered how these varying PV control modes influenced fault currents in the microgrid, providing insights into the effectiveness of the industrial OCR. Figure 23 shows the HIL results for PV control modes A, B, D, and E are matched to the simulation results and time tripping, as presented in Table 8. In the contrast, the OCRs in Control C with significantly low fault, resulting in fault detection difficulties and nontripping and miscoordination events, as shown in Figure 24 and Table 8. These findings further lay much emphasis on the importance of adopting proper PV control strategies that will ensure the optimal operation of OCR and its corresponding times for efficient power system protection.

Overall, when comparing simulated results with real-time testing outcomes for different PV control strategies.

First, simulations using software, ETAP, can model various scenarios and control strategies with high accuracy based on predefined parameters and assumptions. These models allow for extensive testing under controlled conditions, which can provide valuable insights into the theoretical performance of different PV control strategies. Second, real-time testing involves practical equipment and actual fault scenarios, with the Siemens 7SJ631 device and fault injections through OMICRON. This real-time testing provides the opportunity to detect how PV control strategies interact with other system components and external factors that may not be perfectly replicated in simulations. This includes variability in solar irradiance, temperature effects on PV modules, and the impact of network disturbances, which can all influence the performance of the control strategies and the protection devices. The results showed that the OCR with several different types of control, using ETAP software, which is considered one of the most powerful industrial programs. The protection device was also tested practically by using the Siemens 7SJ631 device and fault injection through the OMICRON testing device, and the results were identical. In summary, while simulations provide a valuable theoretical framework for evaluating PV control strategies, real-time testing is crucial for identifying practical

challenges and ensuring that the strategies work effectively in real-world scenarios.

## 5. Conclusions and Recommendations

This paper has investigated the operation of both traditional and nontraditional protection devices under various control strategies in fault conditions. These strategies have evolved significantly in recent years, making it difficult for overcurrent protection devices to detect faults when control types change in certain scenarios. This study verified and analyzed these issues using ETAP software under different operating conditions and fault locations, supplemented by real-time testing using a HIL approach. The OMICRON-256 system facilitated real-time testing on a SIPROTEC 7SJ62 multi-function protection relay. This work has addressed the challenges encountered in the protection system of DNs with IIDGs. By investigating the fault characteristics and fault current contributions from different PV systems under various control strategies, significant insights have been gained. The study emphasizes the influence of control strategies and fault locations on the behavior of IIDG systems during faults, as observed in the 14-bus CIGRE network with two 10 MVA PV farms. The findings highlight the implications of these factors for the coordination and defect detection of OCR protection schemes in evolving power systems. First, the study provides an early exploration of the challenges associated with OCR protection, specifically focusing on the influence of different control techniques employed in PV inverters. This analysis enhances the understanding of OCR protection within the context of evolving power systems, highlighting the need for adapting protection schemes to accommodate the dynamics introduced by IIDGs. Additionally, the investigation by using HIL considers the impact of fault impedance levels on OCR performance under various PV control models and penetration scenarios, including islanded operation. The analysis shows the importance of considering fault impedance variations in achieving optimal coordination and performance of OCRs. Furthermore, optimal coordination schemes utilizing nonstandard and standard tripping characteristics are evaluated and compared under different IIDG control systems. This highlights the limitations of current-only-based fault detection schemes, particularly when control types change. Consequently, this motivates future work to develop methodologies that integrate both current and voltage for fault detection and isolation, ensuring more robust and reliable protection in evolving power system environments, several key points were identified:

- Detection and isolation challenges: OCR may struggle to detect or isolate faults in certain cases, leading to either incorrect disconnections or delays in response times.
- Voltage term in OCR protection: Adding voltage to the OCR scheme may be necessary to effectively detect and isolate faults.
- Comprehensive testing: Extensive testing is required for all types of control methods with other protection

devices, such as distance protection and differential protection, to understand how they detect and isolate faults under various inverter control strategies.

## Nomenclature

OCR:	Overcurrent relay
PV:	Photovoltaic
WCA:	Water cycle optimization algorithm
PSO:	Particle swarm optimization algorithm
SGs:	Synchronous generators
PV:	Photovoltaic
IIDG:	Interconnected inverter-based distributed generation
FRT:	Fault ride-through
SCC:	Short-circuit current computation
DGO:	Distribution grid operator
LVRT:	Low voltage ride-through
RCI:	Reactive current injection
VSI:	Voltage source inverters
$P$ :	Active power
$Q$ :	Reactive power
$V_d$ :	$d$ -axis voltage
$I_{IIDG}$ :	Inverter current
$I_d$ and $I_q$ :	Active and reactive current
$V_{PCC}^+$ :	Positive-sequence voltage
$\Delta V^+$ :	Fault component's voltage
$\Delta I_{IIDG}^+$ :	Fault component's current
$Z_L$ and $Z_S$ :	Line and source impedance
$I_{F1}^+$ :	Fault current at F1
$\Delta I_{R1}^+$ :	Fault current components at OCR1
$R_f$ :	Fault resistance
CTI:	Coordination time Interval
$t_{primary}$ and $t_{backup}$ :	Operational time for both the primary and backup OCRs
TMS:	Time multiplier setting
$t_{min}$ and $t_{max}$ :	Minimum and maximum operational times
$I_p$ :	Pickup current
$t_r$ :	Tripping time
DN:	Distribution network.

## Data Availability Statement

Derived data supporting the findings of this study are available from the corresponding author upon request.

## Ethics Statement

The authors have nothing to report.

## Disclosure

All persons who meet authorship criteria are listed as authors, and all authors certify that they have participated sufficiently in the work to take public responsibility for the content, including participation in the concept, design, analysis, writing, or revision of the manuscript. We also confirm that all



authors have participated in drafting the article or revising it critically for important intellectual content and approval of the final version.

## Conflicts of Interest

The authors declare no conflicts of interest.

## Author Contributions

Conceptualization and project administration: Feras Alasali, Abdelaziz Salah Saidi, and Naser El-Naily. Methodology: Naser El-Naily, Feras Alasali, Emad El Deen Omran, William Holderbaum, and Abdelsalam Elhaffar. Software and formal analysis: Hassen Loukil, Emad El Deen Omran, Feras Alasali, Naser El-Naily, and Abdelaziz Salah Saidi. Validation: all authors. Investigation: Feras Alasali, William Holderbaum, Abdelsalam Elhaffar, and Naser El-Naily. Resources, data curation, writing—review and editing, visualization, and supervision: all authors. Writing—original draft preparation: Feras Alasali, Emad El Deen Omran, and Naser El-Naily. All authors have read and agreed to the published version of the manuscript.

## Funding

The authors extend their appreciation to the Deanship of Research and Graduate Studies at King Khalid University for funding this work through Large Research Project under grant number RGP2/238/45.

## Acknowledgments

We would like to thank Manchester Metropolitan University and The Hashemite University (Renewable Energy Center) for their support in publishing this article.

## References

- [1] A. K. Singh, I. Hussain, and B. Singh, "Double-Stage Three Phase Grid-Integrated Solar PV System With Fast Zero Attracting Normalized Least Mean Forth Based Adaptive Control," *IEEE Transactions on Industrial Electronics* 65, no. 5 (2018): 3921–3931.
- [2] V. Telukunta, J. Pradhan, A. Agrawal, M. Singh, and S. G. Srivani, "Protection Challenges Under Bulk Penetration of Renewable Energy Resources in Power Systems: A Review," *CSEE Journal of Power and Energy Systems* 3, no. 4 (2017): 365–379.
- [3] H. Yazdanpanahi, Y. W. Li, and W. Xu, "A New Control Strategy to Mitigate the Impact of Inverter-Based DGs on Protection System," *IEEE Transactions on Smart Grid* 3, no. 3 (2012): 1427–1436.
- [4] J. Morren and S. W. H. De Haan, "Impact of Distributed Generation Units With Power Electronic Converters on Distribution Network Protection," in *2008 IET 9th International Conference on Developments in Power System Protection (DPSP 2008)*, (IET, 2008): 663–668.
- [5] C. A. Plet, M. Graovac, T. C. Green, and R. Iravani, "Fault Response of Grid-Connected Inverter Dominated Networks," in *IEEE PES General Meeting*, (IEEE, 2010): 1–8.
- [6] H. Hooshyar and M. E. Baran, "Fault Analysis on Distribution Feeders With High Penetration of PV Systems," *IEEE Transactions on Power Systems* 28, no. 3 (2013): 2890–2896.
- [7] F. Katiraei, J. Holbach, T. Chang, et al., "Investigation of Solar PV Inverters Current Contributions During Faults on Distribution and Transmission Systems Interruption Capacity," in *Proceedings of Western Protective Relay Conference* (2012): 1–7, (Washington (DC))
- [8] M. E. Baran and I. El-Markaby, "Fault Analysis on Distribution Feeders With Distributed Generators," *IEEE Transactions on Power Systems* 20, no. 4 (2005): 1757–1764.
- [9] C. A. Plet, M. Graovac, T. C. Green, and R. Iravani, "Fault Response of Grid-Connected Inverter Dominated Networks," in *Proceedings of IEEE Power and Energy Society General Meeting*, (IEEE, 2010): 1–8.
- [10] T. Neumann and I. Erlich, "Short Circuit Current Contribution of a Photovoltaic Power Plant," *IFAC Proceedings Volumes* 45, no. 21 (2012): 343–348.
- [11] P. P. Barker and R. W. De Mello, "Determining the Impact of Distributed Generation on Power Systems. I. Radial Distribution Systems," in *Proceedings of the 2000 Power Engineering Society Summer Meeting*, (IEEE, 2000): 1645–1656.
- [12] M. Meskin, A. Domijan, and I. Grinberg, "Impact of Distributed Generation on the Protection Systems of Distribution Networks: Analysis and Remedies—Review Paper," *IET Generation, Transmission & Distribution* 14, no. 24 (2020): 5944–5960.
- [13] J. Keller and B. Kroposki, *Understanding Fault Characteristics of Inverter-Based Distributed Energy Resources* (Golden, CO, USA: National Renewable Energy Laboratory (NREL), Technical Report, 2010).
- [14] R. C. Dugan and T. E. McDermott, "Distributed Generation," *IEEE Industry Applications Magazine* 8, no. 2 (2002): 19–25.
- [15] M. J. Reno, S. Brahma, A. Bidram, and M. E. Ropp, "Influence of Inverter-Based Resources on Microgrid Protection: Part 1: Microgrids in Radial Distribution Systems," *IEEE Power and Energy Magazine* 19, no. 3 (2021): 36–46.
- [16] S. Manson and E. McCullough, "Practical Microgrid Protection Solutions: Promises and Challenges," *IEEE Power and Energy Magazine* 19, no. 3 (2021): 58–69.
- [17] IEEE Power & Energy Society, "PES-TR67.r1—Impact of IEEE 1547 Standard on Smart Inverters and the Applications in Power Systems," in *IEEE PES Industry Technical Support Leadership Committee*, (IEEE PES, 2020).
- [18] S. Bhagavathy, N. Pearsall, G. Putrus, and S. Walker, "Performance of UK Distribution Networks With Single-Phase PV Systems Under Fault," *International Journal of Electrical Power & Energy Systems* 113 (2019): 713–725.
- [19] X. Kong, Z. Zhang, X. Yin, F. Wang, and M. He, "Study on Fault Current Characteristics and Fault Analysis Method of Power Grid Withinverter Interfaced Distributed Generation," *Zhongguo Dianji Gongcheng Xuebao/Proceedings of the Chinese Society of Electrical Engineering* 33 (2013): 65–74.
- [20] K. Peng, C. Zhang, B. Y. Xu, Y. Chen, J. J. Chen, and X. S. Zhao, "Key Issues of Fault Analysis on Distribution System With High-Density Dis-Tributed Generations," *Automotive Electrical Power System* 41 (2017): 184–192.
- [21] X. Shi, H. Zhang, C. Wei, Z. Li, and S. Chen, "Fault Modeling of IIDG Considering Inverter's Detailed Characteristics," *IEEE Access* 8 (2020): 183401–183410.
- [22] L. V. Strezoski, B. Dumnicek, B. Popadic, M. Prica, and K. A. Loparo, "Novel Fault Models for Electronically Coupled Distributed Energy Resources and Their Laboratory Validation," *IEEE Transactions on Power Systems* 35, no. 2 (2020): 1209–1217.



- [23] K. H. Oon, C. K. Tan, A. H. A. Bakar, H. S. Che, H. Mokhlis, and H. A. Illias, "Establishment of Fault Current Characteristics for Solar Photovoltaic Generator Considering Low Voltageride Through and Reactive Current Injection Requirement," *Renewable and Sustainable Energy Reviews* 92 (2018): 478–488.
- [24] IEC 60909-0, "Short-Circuit Currents in Three-Phase a.c. Systems, Part 0: Calculation of Currents, First Edition," (2001).
- [25] IEC 60909-0, "Short-circuit Currents in Three-Phase a.c. Systems, Part 0: Calculation of Currents," (2016).
- [26] D. Ghaderi, Gökay Bayrak, and J. M. Guerrero, "Grid Code Compatibility and Real-Time Performance Analysis of an Efficient Inverter Topology for PV-Based Microgrid Applications," *International Journal of Electrical Power & Energy Systems* 128 (2021): 106712.
- [27] Y. Liu, Y. Wang, H. Liu, et al., "An LVRT Strategy With Quantitative Design of Virtual Impedance for VSG," *International Journal of Electrical Power & Energy Systems* 140 (2022): 107661.
- [28] A. Haddadi, M. Zhao, I. Kocar, U. Karaagac, K. W. Chan, and E. Farantatos, "Impact of Inverter-Based Resources on Negative Sequence Quantities-Based Protection Elements," *IEEE Transactions on Power Delivery* 36, no. 1 (2021): 289–298.
- [29] A. Haddadi, I. Kocar, et al., *Impact of Inverter-Based Resources on Protection Schemes Based on Negative Sequence Components* (Palo Alto, CA: EPRI, 2019).
- [30] L. Kong and H. Nian, "Fault Detection and Location Method for Mesh-Type DC Microgrid Using Pearson Correlation Coefficient," *IEEE Transactions on Power Delivery* 36, no. 3 (2021): 1428–1439.
- [31] B. Mahamedi and J. E. Fletcher, "Trends in the Protection of Inverter-Based Microgrids," *IET Generation, Transmission & Distribution* 13, no. 20 (2019): 4511–4522.
- [32] F. Alasali, N. El-Naily, E. Zarour, and S. M. Saad, "Highly Sensitive and Fast Microgrid Protection Using Optimal Coordination Scheme and Nonstandard Tripping Characteristics," *International Journal of Electrical Power & Energy Systems* 128 (2021): 106756.
- [33] R. Sitharthan, M. Geethanjali, and T. Karpaga Senthil Pandey, "Adaptive Protection Scheme for Smart Microgrid With Electronically Coupled Distributed Generations," *Alexandria Engineering Journal* 55, no. 3 (2016): 2539–2550.
- [34] W. K. A. Najy, H. H. Zeineldin, and W. L. Woon, "Optimal Protection Coordination for Microgrids With Grid-Connected and Islanded Capability," *IEEE Transactions on Industrial Electronics* 60, no. 4 (2013): 1668–1677.
- [35] G. Ameen, M. Elmusrati, and A. Gaouda, "Enhancing the Operation of Smart Inverters With PMU and Data Concentrators," *International Journal of Electrical Power & Energy Systems* 140 (2022): 108077.
- [36] F. Rohde and S. Hielscher, "Smart Grids and Institutional Change: Emerging Contestations Between Organisations Over Smart Energy Transitions," *Energy Research & Social Science* 74 (2021): 101974.
- [37] IEC 60909-0:2001, "Short-Circuit Currents in Three-Phase A. C. Systems—Part 0: Calculation of Currents," Calculation of Currents (2001).
- [38] IEEE Standards Association. 242-2001, "IEEE Recommended Practice for Protection and Coordination of Industrial and Commercial Power Systems (ANSI)," (2001).
- [39] T. S. Basso and R. DeBlasio, "IEEE 1547 Series of Standards: Interconnection Issues," in *IEEE Transactions on Power Electronics*, 19, no. 5, (IEEE, 2004): 1159–1162.
- [40] N. Nimpitiwan, G. T. Heydt, R. Ayyanar, and S. Suryanarayanan, "Fault Current Contribution From Synchronous Machine and Inverter Based Distributed Generators," in *IEEE Transactions on Power Delivery*, 22, no. 1, (IEEE, 2006): 634–641.
- [41] C. Schauder, "Impact of FERC 661-A and IEEE. 1547 on Photovoltaic Inverter Design," in *2011 IEEE Power and Energy Society General Meeting*, (IEEE, 2011): 1–6.
- [42] International Electrotechnical Commission (IEC), "Short-Circuit Currents in Three-phase a.c. Systems—Part 0: Calculation of Currents (IEC 60909-0: 2016)," Technical report, IEC, p. 149p. 149, 2016.
- [43] IEEE Industry Applications Society, "Std3002.3-IEEE Recommended Practice for Conducting Short-Circuit Studies and Analysis of Industrial and Commercial Power Systems," (2018).
- [44] IEEE Std 1547-2018, *IEEE Standard for Interconnection and Interoperability of Distributed Energy Resources With Associated Electric Power Systems Interfaces* (Piscataway, NJ, USA: IEEE, 2018): 1–138.
- [45] R. Aljarrah, H. Marzooghi, V. Terzija, and J. Yu, "Modifying IEC 60909 Standard to Consider Fault Contribution From Renewable Energy Resources Utilizing Fully-Rated Converters," in *2019 9th International Conference on Power and Energy Systems (ICPES)* (2019): 1–6
- [46] IEC TR 60909-4, "Short-Circuit Currents in Three-Phase a.c. Systems, Part 4: Examples for the Calculation of Short-Circuit Currents," (2021).
- [47] Y. Li and D. Wang, "Asymmetrical Fault Analysis on Distribution Feeders With Inverter Interfaced Distributed Generators," *International Journal of Electrical Power & Energy Systems* 125 (2021): 106514.
- [48] I. Kim, "A Calculation Method for the Short-Circuit Current Contribution of Current-Control Inverter-Based Distributed Generation Sources at Balanced Conditions," *Electric Power Systems Research* 190 (2021).
- [49] IEEE Std 2800-2022, "IEEE Standard for Interconnection and Interoperability of Inverter-Based Resources (IBRs) Interconnecting With Associated Transmission Electric Power Systems," (IEEE, 2022): 1–180.
- [50] T. R. Mabote, J. E. Tabarez, A. K. Barnes, A. Mate, R. W. Bent, and E. Cotilla-Sanchez, "Developing Optimization-Based Inverter Models for Short Circuit," arXiv preprint arXiv:2305.00804 (2023).
- [51] M. J. Davi, M. Oleskovicz, and F. V. Lopes, "Study on IEEE 2800-2022 Standard Benefits for Transmission Line Protection in the Presence of Inverter-Based Resources," *Electric Power Systems Research* 220 (2023).
- [52] N. Chang, G. Song, J. Hou, and Z. Chang, "Fault Identification Method Based on Unified Inverse-Time Characteristic Equation for Distribution," *International Journal of Electrical Power & Energy Systems* 146 (2023): 108734.
- [53] M.-A. Nasr and A. Hooshyar, "Controlling Grid-Forming Inverters to Meet the Negative-Sequence Current Requirements of the IEEE Standard 2800-2022," *IEEE Transactions on Power Delivery* 38, no. 4 (2023): 2541–2555.
- [54] L. V. Strezoski and N. G. Simic, "Quantifying the Impact of Inverter-Based Distributed Energy Resource Modeling on Calculated Fault Current Flow in Microgrids," *International Journal of Electrical Power & Energy Systems* 151 (2023): 109161.
- [55] X. Miao, D. Zhao, B. Lin, H. Jiang, and J. Chen, "A Differential Protection Scheme Based on Improved DTW Algorithm for Distribution Networks With Highly-Penetrated Distributed Generation," *IEEE Access* 11 (2023): 40399–40411.

- [56] S. Hester, "IEEE 929-2000 Recommended Practice for Utility Interface of Photovoltaic (PV) Systems," in *Workshop Proceedings-Solar Electric Power Association*, (IEEE, 2000).
- [57] M. Ghotbi-Maleki, R. M. Chabanloo, H. H. Zeineldin, and S. M. H. Miangafsheh, "Design of Setting Group-Based Overcurrent Protection Scheme for Active Distribution Networks Using MILP," *IEEE Transactions on Smart Grid* 12, no. 2 (2021): 1185–1193.
- [58] M. C. Vargas, O. E. Batista, and Y. Yang, "Estimation Method of Short-Circuit Current Contribution of Inverter-Based Resources for Symmetrical Faults," *Energies* 16, no. 7 (2023): 3130.
- [59] E. Zarour, F. Alasali, O. Alsmadi, and N. El-Naily, "A New Adaptive Protection Approach for Overcurrent Relays Using Novel Nonstandard Current-Voltage Characteristics," *Electric Power Systems Research* 216 (2023): 109083.
- [60] N. El-Naily, S. Saad, A. Elhaffar, E. Zarour, and F. Alasali, "Innovative Adaptive Protection Approach to Maximize the Security and Performance of Phase/Earth Overcurrent Relay for Microgrid Considering Earth Fault Scenarios," *Electric Power Systems Research* 206 (2022): 107844.
- [61] S. Saldarriaga-Zuluaga, J. A. López-Lezama, and N. Muñoz-Galeano, "Optimal Coordination of Overcurrent Relays in Microgrids Considering a Non-Standard Characteristic," *Energies* 13, no. 4 (2020): 922.
- [62] A. Sadollah, H. Eskandar, and J. H. Kim, "Water Cycle Algorithm for Solving Constrained Multi-Objective Optimization Problems," *Applied Soft Computing* 27 (2015): 279–298.
- [63] J.-B. Park, K.-S. Lee, J.-R. Shin, and K. Y. Lee, "A Particle Swarm Optimization for Economic Dispatch With Non-smooth Cost Functions," *IEEE Transactions on Power Systems* 20, no. 1 (2005): 34–42.
- [64] e-cigre, "Benchmark Systems for Network Integration of Renewable and Distributed Energy Resources," 2014, [https://e-cigre.org/publication/ELT\\_273\\_8-benchmark-systems-for-network-integration-of-renewable-and-distributedenergy](https://e-cigre.org/publication/ELT_273_8-benchmark-systems-for-network-integration-of-renewable-and-distributedenergy).